# HCV infection activates the proteasome via PA28γ acetylation and heptamerization to facilitate the degradation of RNF2, a catalytic component of polycomb repressive complex 1.

Hirotake Kasai[1], Atsuya Yamashita[1], Yasunori Akaike[1], Tomohisa Tanaka[1, 4], Yoshiharu Matsuura[2, 3], and Kohji Moriishi[1, 4].

[1] Department of Microbiology, Faculty of Medicine, Graduate Faculty of Interdisciplinary Research, University of Yamanashi, Yamanashi 409-3898, Japan.
[2] Laboratory of Virus Control, Research Institute for Microbial Diseases (RIMD), Osaka University, Osaka 565-0871, Japan.
[3] Center for Infectious Diseases Education and Research (CiDER), Osaka University, Osaka 565-0871, Japan.
[4] Division of Hepatitis Virology, Institute for Genetic Medicine, Hokkaido University, Hokkaido 060-0808, Japan

**ABSTRACT**

We previously reported that hepatitis C virus (HCV) infection or HCV core protein expression induces HOX gene expression by impairing histone H2A monoubiquitination via a proteasome-dependent reduction in the level of RNF2, a key catalytic component of polycomb repressive complex 1 (PRC1) (J. Virol, 2021, 95, e01784-20). In this study, we aimed to investigate the mechanism by which HCV infection accelerates RNF2 degradation. Yeast two-hybrid screening and an immunoprecipitation assay revealed that RNF2 is a PA28γ-binding protein. The proteasome activator PA28γ destabilized the RNF2 protein in a proteasome-dependent manner, since RNF2 degradation was impaired by PA28γ knockout or MG132 treatment. HCV infection or core protein expression reduced the levels of RNF2 and histone H2A K119 monoubiquitination and induced the expression of HOX genes in the presence of PA28γ, while PA28γ knockout reversed these changes. Treatment with a lysine acetyltransferase inhibitor inhibited the acetylation of PA28γ at K195 and the degradation of the RNF2 protein, while treatment with a lysine deacetylase inhibitor accelerated these events in a PA28γ-dependent manner. RNF2 protein degradation was increased by expression of the acetylation mimetic PA28γ mutant but not by expression of the acetylation-defective mutant or the proteasome activation-defective mutant. Furthermore, HCV infection or core protein expression facilitated the interaction between PA28γ and the lysine acetyltransferase CBP/p300 and then accelerated PA28γ acetylation and heptamerization to promote RNF2 degradation. These data suggest that HCV infection accelerates the acetylation-dependent heptamerization of PA28γ to increase the proteasomal targeting of RNF2.

**IMPORTANCE**: HCV is a causative agent of HCV-related liver diseases, including hepatic steatosis, cirrhosis and hepatocellular carcinoma. PA28γ, which, in heptameric form, activates the 20S core proteasome for the degradation of PA28γ-binding proteins, is responsible for HCV-related liver diseases. HCV core protein expression or HCV infection accelerates RNF2 degradation, leading to the induction of HOX gene expression via a decrease in the level of H2Aub on HOX gene promoters. However, the mechanism of RNF2 degradation in HCV-infected cells has not been clarified. The data presented in this study suggest that PA28γ acetylation and heptamerization are promoted by HCV infection or by core protein expression to activate the proteasome for the degradation of RNF2 and are responsible for HCV propagation. This study provides

52 novel insights valuable for the development of therapies targeting both HCV
53 propagation and HCV-related diseases.
54
55 **KEYWORDS: HCV, RNF2, H2A monoubiquitination, PA28γ/REGγ/PMSE3/Ki**
56
57 **INTRODUCTION**
58 Hepatitis C virus (HCV) is a major human pathogen that is currently causing chronic
59 infection in 50 million people worldwide, with approximately 1.0 million new
60 infections occurring annually, and puts infected individuals at risk of hepatic steatosis,
61 liver cirrhosis, and hepatocellular carcinoma (HCC) (1). The development of direct-
62 acting antiviral agents (DAAs) against HCV has led to significant improvements in the
63 treatment of HCV infections over the past decade (2, 3). However, it has also been
64 reported that hepatitis C patients remain at risk of HCC even after viral elimination (2).
65 Understanding the pathogenesis of HCV infection remains an important challenge for
66 the development of effective hepatitis C therapies. HCV belongs to the genus
67 *Hepacivirus* in the *Flaviviridae* family and possesses an enveloped nucleocapsid
68 containing a positive-sense RNA genome with a length of 9.6 kb. The single
69 polyprotein (~ 3000 amino acids) encoded by the viral genome is cleaved by viral and
70 host proteases into 10 final viral proteins, which are classified as structural or
71 nonstructural proteins (4). The structural proteins are the core, E1 and E2 proteins, and
72 the nonstructural proteins are the p7, NS2, NS3, NS4A, NS4B, NS5A, and NS5B
73 proteins. Nonstructural proteins play important roles in viral genome replication,
74 assembly, and budding, whereas structural proteins, together with the host lipid bilayer,
75 form viral particles (4). The core protein, a component of the nucleocapsid, has been
76 implicated in the formation of viral particles as well as the induction of HCV-related
77 pathological changes (4). Mice expressing the core protein in the liver were found to
78 exhibit HCV-related liver diseases such as type II diabetes mellitus (5), hepatic steatosis
79 (6, 7), and HCC (8, 9), suggesting that the core protein plays an important role in
80 inducing HCV-related pathological changes.
81 We previously reported that the HCV core protein can promote a reduction in the
82 monoubiquitination of lysine (K) 119 of histone H2A in the promoter regions of HOX
83 alleles and subsequently activate the transcription of HOX genes (10). HOX family
84 genes, a set of 39 genes divided into 4 clusters, namely, HOXA, HOXB, HOXC and

85 HOXD, regulate body plan development during the neonatal stage and also regulate the
86 growth, survival, migration and invasion of cells to support cancer development (11,
87 12). Monoubiquitination of H2A at K119 is catalysed by polycomb repressive complex
88 1 (PRC1) to repress target genes (13). The expression of the HCV core protein was
89 found to increase the degradation of the RNF2 protein, a main catalytic component of
90 PRC1, and reduce the level of K119-monoubiquitinated histone H2A (H2Aub) on the
91 promoter regions of HOX alleles (10). The core protein-dependent degradation of RNF2
92 was found to be independent of polyubiquitination and to be inhibited by treatment with
93 the proteasome inhibitor MG132 (10). However, the molecular mechanism by which the
94 core protein induces polyubiquitination-independent, proteasome-dependent
95 degradation of RNF2 remains unclear.
96 The ubiquitin–proteasome system is a major proteolytic pathway that regulates
97 various intracellular functions. The proteasome complex consists of the 20S proteolytic
98 core and several proteasome activators (PAs), including the 19S PA (PA700), 11S PA
99 (PA28 or REG), and PA200. The 19S PA can bind to the 20S proteasome and activate
100 polyubiquitination-dependent proteolysis (14), while the 11S PA can bind to the 20S
101 proteasome and activate polyubiquitin-independent proteolysis (14). The 11S PA is
102 classified as a PA28α/PA28β heteroheptamer or a PA28γ homoheptamer. The
103 expression of PA28α and PA28β is induced by interferon (IFN)-γ for the processing of
104 MHC class I peptides (14). The PA28α/PA28β heteroheptamer activates the
105 chymotrypsin-like activity of the 20S core proteasome (CP) in the cytoplasm, while the
106 PA28γ homoheptamer activates the trypsin-like activity of the 20S CP in the nucleus
107 (15). Several proteins, such as AID, SRC-3, p19, the HCV core protein and SirT1, have
108 been reported to be substrates of the PA28γ-dependent proteasome system (4, 16-18).
109 The amino acid sequence of human PA28γ is identical to that of its murine homologue
110 and shares 55% identity with that of its tick homologue (19), suggesting that PA28γ is
111 highly conserved from insects to mammals. This broad conservation indicates that
112 PA28γ may regulate fundamental functions across the animal kingdom, although its
113 detailed biological function is largely unknown. We previously reported that PA28γ
114 binds to the HCV core protein and promotes the degradation of unfolded or
115 nonfunctional core proteins through a polyubiquitin-independent proteosomal pathway
116 (20, 21). Furthermore, PA28γ knockout abolished core protein-related liver defects
117 (type II diabetes, steatosis, and HCC) in mice, suggesting that PA28γ plays a critical

118 role in core protein-induced pathological changes (22, 23). Phenotypic analysis of
119 PA28γ-knockout mice revealed that they were viable and capable of mating but
120 exhibited mild growth defects (24), decreased sperm fertility (25), and accelerated
121 senescence (26), although a critical function of PA28γ has not yet been identified.
122 In this study, we identified RNF2 as a novel PA28γ-binding protein and
123 examined the effect of PA28γ on the stability of RNF2, monoubiquitination of histone
124 H2A, regulation of HOX gene transcription, and propagation of HCV. We also aimed to
125 clarify the mechanism by which the HCV core protein regulates PA28γ-dependent
126 proteasome activity to inhibit PRC1 activity in HCV-infected cells.
127
128 **RESULTS**
129 **PA28γ interacted with RNF1 and RNF2, components of polycomb repressor**
130 **complex 1.**
131 To identify novel PA28γ-binding molecules, we screened a human foetal brain library
132 using a yeast two-hybrid system with PA28γ as bait. RNF1, a component of PRC1, was
133 identified as a PA28γ-binding partner by this yeast two-hybrid screen. Since RNF2 is a
134 catalytic component of PRC1 and is a homologue of RNF1, the RNF2 gene was isolated
135 from total cDNA of the human liver. Plasmids encoding N-terminal FLAG-tagged
136 PA28γ (FLAG-PA28γ), N-terminal HA-tagged RNF1 (HA-RNF1) and N-terminal HA-
137 tagged RNF2 (HA-RNF2) were constructed to examine the interactions of PA28γ with
138 RNF1 and RNF2 by immunoprecipitation in 293T cells. HA-RNF1 or HA-RNF2 was
139 coimmunoprecipitated with FLAG-PA28γ, while FLAG-PA28γ was reciprocally
140 coimmunoprecipitated with HA-RNF1 or HA-RNF2 (Fig. 1A). Next, we examined the
141 subcellular localization of PA28γ and RNF2 by immunofluorescence staining.
142 Unfortunately, we could not find an antibody that reacts specifically with endogenous
143 RNF1. However, PA28γ and RNF2 were partially colocalized in the nucleus (Fig. 1B).
144 The fluorescence intensities of PA28γ (green) and RNF2 (red) within each pixel were
145 quantified and plotted (Fig. 1C), revealing a negative correlation for the colocalization
146 of these two proteins (R = -0.856, Fig. 1C). These data suggest that PA28γ binds to
147 RNF2 but is not strongly colocalized with RNF2 in untreated cells.
148
149 **PA28γ reduced the stability of RNF1 and RNF2**

150 We hypothesized that the intracellular segregation of PA28γ and RNF2 may be
151 due to PA28γ-dependent degradation of RNF2 following the interaction between these
152 two proteins, because PA28γ-binding proteins are reportedly degraded via a
153 polyubiquitin-independent proteosomal pathway (15). Using the CRISPR-Cas9 system,
154 we established a PA28γ-knockout cell line and then examined the stability of the RNF1
155 and RNF2 proteins via a cycloheximide (CHX) chase assay. PA28γ was detected in
156 wild-type Huh7OK1 cells, which are highly permissive to HCV infection (27), but not
157 in PA28γ-knockout Huh7OK1 cells (Fig. 2A, B). The level of RNF2 in the wild-type
158 cells was reduced by less than 50% 2 h after CHX treatment, whereas no significant
159 reduction in the RNF2 level was observed in the PA28γ-knockout cells (Fig. 2A, B).
160 RNF1 tended to be less stable in PA28γ-knockout cells than in wild-type cells, but the
161 difference was not significant (Fig. 2A, B). In addition, the stability of BMI1 (PCGF4),
162 another component of PRC1, was not affected by PA28γ knockout (Fig. 2A, B). These
163 data suggest that PA28γ destabilizes RNF2.
164 When PA28γ expression was restored in PA28γ-knockout cells, the
165 endogenous RNF1 and RNF2 protein levels decreased in a PA28γ dose-dependent
166 manner (Fig. 3A). However, the RNF1 and RNF2 mRNA levels were not affected by
167 restoration of PA28γ expression (Fig. 3B). Furthermore, restoring the expression of
168 PA28γ reduced the levels of HA-RNF1 and HA-RNF2 (Fig. 3C). HA-RNF1 and HA-
169 RNF2 was expressed separately in 293T cells and were then isolated by
170 immunoprecipitation using an anti-HA antibody for *in vitro* proteasome assays. The
171 immunoprecipitates containing HA-RNF1 or HA-RNF2 were mixed with recombinant
172 20S CP with or without the 11S PA consisting of PA28γ. The levels of HA-RNF1 and
173 HA-RNF2 were reduced in the presence but not in the absence of the 11S PA. These
174 results suggest that PA28γ is involved in the proteolysis of RNF1 and RNF2. Since the
175 RNF2 protein was more strongly destabilized by PA28γ than was the RNF1 protein, we
176 subsequently focused on the relationship between RNF2 and PA28γ.
177
178 **PA28γ promoted proteasome-dependent degradation of the RNF2 protein.**
179 PA28γ increases the trypsin-like activity of the ubiquitin-independent proteasome. We
180 next examined the effect of proteasome activity on RNF2 stability in the presence of
181 PA28γ. The RNF2 protein level was reduced in PA28γ-knockout cells by restoration of
182 PA28γ expression, while MG132 treatment suppressed the PA28γ-dependent decrease

183 in the RNF2 protein level (Fig. 4A). The intracellular localization of PA28γ and RNF2
184 was evaluated in the presence and absence of MG132. RNF2 was partially colocalized
185 with PA28γ in the absence of MG132, while it strongly colocalized with PA28γ in the
186 presence of MG132 (Fig. 4B). A negative correlation for the colocalization of wild-type
187 PA28γ and RNF2 was found in the cells (Fig. 4C, a left half). The PA28γ mutant in
188 which proline 245 (Pro245) was replaced with tyrosine (Tyr; PA28γP245Y) could not
189 activate the proteasome (21, 28). The colocalization of PA28γP245Y and RNF2 was
190 positively correlated in the cells (Fig. 4C, a right half). These data suggest that PA28γ
191 promotes the proteolytic degradation of RNF2 in a proteasome-dependent manner.
192
193 **PA28γ impaired the monoubiquitination of histone H2A at K119 and induced the**
194 **transcription of HOX genes.**
195 PRC1 monoubiquitinates K119 of histone H2A to suppress the transcription of target
196 genes via chromatin compaction (13, 29). RNF2 is an E3 ubiquitin ligase responsible
197 for the catalytic activity of PRC1 for the monoubiquitination of histone H2A at K119
198 (13, 30, 31). We next examined the effects of PA28γ expression on histone H2A
199 monoubiquitination and on the transcription of HOX genes. Restoration of PA28γ
200 expression reduced the level of H2Aub (Fig. 5A) in PA28γ-knockout cells but did not
201 affect the level of total histone H2A. We previously reported that HOXB9, HOXC13,
202 and HOXD13 were completely silenced in Huh7OK1 cells but HOXA1 and HOXA3
203 was not (10). We evaluated the effect of PA28γ expression on the expression of the
204 group with HOX gene silencing. Restoring the expression of PA28γ in PA28γ-knockout
205 cells induced the transcriptional activation of HOXB9 (Fig. 5B). The level of H2Aub in
206 the promoter region of HOXB9 was then evaluated by a chromatin immunoprecipitation
207 (ChIP) assay and was found to be reduced by the restoration of PA28γ expression in
208 PA28γ-knockout cells (Fig. 5C). The HOXB1, HOXC13 and HOXD13 genes were also
209 transcriptionally activated by PA28γ expression (Fig. 5D), whereas HOXA1 and
210 HOXA3 gene transcription was not affected by the restoration of PA28γ expression in
211 PA28γ-knockout cells (Fig. 5D). These data suggest that PA28γ reactivates the
212 expression of silenced HOX genes via impairment of H2A monoubiquitination.
213
214 **HCV infection impaired the monoubiquitination of histone H2A at K119 and**
215 **reduced the level of RNF2 in a PA28γ-dependent manner.**

216 We previously showed that HCV infection promoted RNF2 protein degradation via a
217 polyubiquitination-independent proteasome pathway and subsequently reduced the level
218 of H2Aub in the promoter regions of HOX genes (10). When wild-type Huh7OK1 cells
219 were infected with HCV, the levels of H2Aub and RNF2 were reduced in a manner
220 dependent on the number of days after infection in the presence but not in the absence
221 of PA28γ (Fig. 6A, B). Knocking out PA28γ did not affect HCV replication, although it
222 increased the level of the HCV core protein in cells and reduced the levels of both HCV
223 RNA and infectious viral particles in the culture supernatant (Fig. 6C), consistent with
224 the data shown in our previous report (21). These findings suggest that HCV infection
225 impairs the monoubiquitination of histone H2A and the stability of RNF2 in a PA28γ-
226 dependent manner.
227
228 **The HCV core protein reduced the level of H2Aub in the promoter regions of**
229 **HOX genes and promoted their transcription in the presence but not in the**
230 **absence of PA28γ.**
231 Our previous report suggested that polyubiquitination-independent proteolysis of
232 RNF2 is promoted by the expression of the HCV core protein to activate HOX gene
233 transcription in HCV-infected cells (10). Next, we examined whether the expression of
234 the HCV core protein affects the RNF2 protein level, the H2A monoubiquitination level
235 and HOX gene transcription in the presence or absence of PA28γ. Expression of the
236 core protein reduced the levels of H2Aub and RNF2 in the presence but not in the
237 absence of PA28γ, although the level of the core protein was markedly higher in
238 PA28γ-knockout cells than in wild-type cells (Fig. 7A). A ChIP assay was carried out to
239 estimate the level of H2Aub in the HOXB9 promoter region. The level of H2Aub in the
240 HOXB9 promoter region was reduced by expression of the core protein in the presence
241 but not in the absence of PA28γ (Fig. 7B). On the other hand, core protein expression
242 promoted the transcription of the HOXB9 gene in the presence but not in the absence of
243 PA28γ (Fig. 7C). These data suggest that the core protein reduces the levels of RNF2
244 and H2Aub and increases the expression of HOX gene in the presence but not in the
245 absence of PA28γ.
246
247 **Acetylation of PA28γ at Lys195 promoted its homoheptamerization and RNF2**
248 **degradation.**

249 PA28γ was reported to be acetylated at Lys195 (K195) to promote its
250 homoheptamerization for 20S CP binding and proteasome activation (32). CBP/p300, a
251 lysine acetyltransferase (KAT), was reported to be responsible for the acetylation of
252 PA28γ at K195 (32). Moreover, the core protein can interact with CBP and increase its
253 acetyltransferase activity (33). We hypothesized that the core protein promotes CBP-
254 dependent acetylation of PA28γ and augments the homoheptamerization of PA28γ to
255 activate the proteasome to target RNF2 for degradation. We examined the effect of the
256 KAT inhibitor C646 on PA28γ-dependent RNF2 degradation. Restoring the expression
257 of PA28γ reduced the RNF2 level in PA28γ-knockout cells; in addition, CHX treatment
258 promoted the reduction in the RNF2 level in the presence of PA28γ, whereas C646
259 treatment impaired the reduction in the RNF2 level in the presence of PA28γ regardless
260 of CHX treatment (Fig. 8A). Immunoprecipitation using an anti-acetylated lysine (Ace-
261 K) antibody and the lysates used to acquire the data shown in Fig. 8A showed that C646
262 treatment suppressed PA28γ acetylation (Fig. 8B). On the other hand, treatment with the
263 lysine deacetylase inhibitor trichostatin A (TSA) promoted the decrease in the RNF2
264 level in the presence but not in the absence of PA28γ (Fig. 8C), while TSA treatment
265 increased PA28γ acetylation (Fig. 8D). PA28γK195R, in which Lys195 is replaced with
266 Arg, is an acetylation-defective mutant, while PA28γK195Q, in which Lys195 is
267 replaced with Gln, is an acetylation mimetic mutant (32). A CHX chase assay was
268 carried out to investigate the stability of RNF2 in the presence of wild-type PA28γ or
269 these mutants. Six hours after treatment with CHX, the RNF2 level was 21% of that in
270 the control cells in the cells expressing wild-type PA28γ, 104% of that in the control
271 cells in the cells expressing PA28γK195R and 14% of that in the control cells in the
272 cells expressing PA28γK195Q. These results suggest that the regulation of PA28γ
273 acetylation is controls the PA28γ-dependent degradation of RNF2. The HCV core
274 protein increased the degradation of RNF2 in the absence but not in the presence of
275 C646, suggesting that the core protein promotes the PA28γ-dependent degradation of
276 RNF2 via KAT activation. These data suggest that HCV infection or the core protein
277 expression promotes PA28γ acetylation for destabilization of RNF2.
278
279 **HCV infection promoted the acetylation of PA28γ via CBP activity.**
280 We investigated the mechanism by which HCV infection or core protein expression
281 promotes PA28γ acetylation. Huh7OK1 cells were infected with HCV, and the infected

282 cells were harvested at 0, 3 and 6 dpi. The cell lysates were subjected to
283 immunoprecipitation using rabbit anti-Ace-K IgG or normal rabbit IgG. The levels of
284 acetylated PA28γ and PA28γ homoheptamers increased in a time-dependent manner
285 after infection (Fig. 9A, B). When PA28γ expression was restored with or without the
286 expression of the core protein in PA28γ-knockout cells, the core protein promoted
287 PA28γ acetylation and homoheptamerization (Fig. 9B, C), consistent with the data
288 shown in Fig. 9A. The core protein has been reported to interact with CBP and
289 subsequently increase its acetyltransferase activity (33). EGFP-PA28γ and FLAG-CBP
290 were coexpressed in PA28γ-knockout cells, and EGFP-PA28γ coimmunoprecipitated
291 with FLAG-CBP (lane 4, Fig. 9D). Furthermore, the core protein increased the amount
292 of EGFP-PA28γ coimmunoprecipitated with CBP (lane 5, Fig. 9D). The RNF2 protein
293 level was decreased in HCV-infected cells but was restored by CBP knockdown in
294 infected cells (Fig. 9E). Taken together, these results suggest that the HCV core protein
295 in infected cells reinforces the interaction between PA28γ and CBP, induces the
296 acetylation and homoheptamerization of PA28γ, and activates the proteasome for RNF2
297 degradation.
298
299 **DISCUSSION**
300 Alterations in gene expression patterns in HCV-infected cells or liver tissue
301 of individuals with hepatitis C may be involved in the pathogenic mechanism of HCV
302 (34). We previously reported that HCV infection impaired PRC1-dependent
303 monoubiquitination of histone H2A at K119 on HOX alleles through degradation of
304 RNF2, which subsequently induced the expression of HOX genes (10). The data in this
305 previous report also suggested that RNF2, a catalytic component of PRC1, is degraded
306 in response to HCV infection or core protein expression and that this degradation is
307 dependent on the proteasome but not on polyubiquitination (10). However, the
308 mechanism by which the core protein induces the degradation of RNF2 after infection
309 has not been elucidated. Furthermore, we previously reported that PA28γ is responsible
310 for the core protein-related pathological changes. The PA28 family members, namely,
311 α, β and γ, form heptamers that bind to the 20S proteasome and then stimulate
312 polyubiquitin-independent proteasome activity. The PA28γ homoheptamer activates the
313 20S CP for the degradation of PA28γ-binding proteins. In mice, HCV core protein
314 expression induces the development of hepatic steatosis, HCC and type II diabetes

315 mellitus (5, 9, 23), which are highly prevalent in hepatitis C patients (35), and these core
316 protein-related pathological conditions are reversed by PA28γ knockout in mice (22,
317 23). The data presented in our previous study also suggest that PA28γ binds the core
318 protein and then induces the degradation of the unfolded core protein to promote viral
319 particle production (20, 21). However, the mechanism by which the core protein
320 induces HCV-related pathological changes via a PA28γ-related pathway remains
321 unknown. In this study, the results of the yeast two-hybrid screen using PA28γ as bait
322 revealed that RNF1 and RNF2 were the candidate PA28γ-binding partners. PA28γ
323 bound both RNF1 and RNF2 (Fig. 1) and accelerated RNF2 degradation but only
324 weakly affected RNF1 degradation, leading to the upregulation of HOX gene
325 expression (Figs. 2 to 5). Furthermore, PA28γ promoted the proteasome-dependent
326 degradation of RNF2 to impair the monoubiquitination of histone H2A (Figs. 4 to 6).
327 Liu et al reported that CBP-induced acetylation of PA28γ at K195 resulted in
328 homoheptamerization of PA28γ and subsequently stimulated polyubiquitin-independent
329 proteasome activity (32). The data shown in Figs. 8 and 9 support the idea that CBP-
330 dependent acetylation of PA28γ leads to heptamerization of PA28γ (Fig. 8) and suggest
331 that core protein expression promotes the acetylation of PA28γ via CBP activity in
332 infected cells (Fig. 9). Taken together, these data suggest that after HCV infection, the
333 core protein reinforces the interaction between CBP and PA28γ, induces PA28γ
334 heptamerization, and subsequently stimulates polyubiquitin-independent proteasome
335 activity for RNF2 protein degradation. The data presented in this study also suggest that
336 PA28γ expression is required for the reduction in H2Aub in HCV-infected cells.
337 Identifying the other loci and genomic regions at which PA28γ reduces the level of
338 H2Aub is an important and challenging task necessary for understanding the
339 physiological and pathological functions of PA28γ in hepatitis C pathogenesis. A model
340 of the mechanism by which HCV infection facilitates the degradation of RNF2 via a
341 PA28γ-dependent proteasome pathway to impair histone H2A monoubiquitination and
342 induce HOX gene expression is shown in Fig. 10.
343 Several reports indicate that the core protein promotes the degradation of p21
344 (36, 37), whereas other reports suggest that the core protein induces G1 arrest after
345 common bile duct ligation, alters the cell cycle in hepatocytes and is associated with
346 increased p21 expression (38). PA28γ was reported to bind cyclin kinase inhibitors,
347 such as p21 and p19, to promote their degradation via the PA28γ-20S CP complex and

348 then to induce S phase entry (18, 39). These observations and the data presented in the
349 current study suggest that the core protein may regulate the cell cycle via the control of
350 the PA28γ-dependent proteasome. In addition, HOX protein expression induced by the
351 core protein may promote the transcriptional activation of genes associated with
352 degradation of cell cycle inhibitors. HOXA10 overexpression was reported to promote
353 the expression of S-phase kinase-associated protein 2 (SKP2), which contributes to the
354 degradation of the cell cycle inhibitor p27 (40). The upregulation of HOX gene
355 expression in HCV-infected hepatocytes may be associated with the promotion of cell
356 cycle progression via transcriptional and/or posttranslational regulation of cell cycle
357 inhibitors.
358 The induction of HOX genes may contribute to carcinogenesis by regulating
359 cell growth, survival, migration and invasion in addition to regulating the cell cycle.
360 Several HOX genes have been reported to be dysregulated in a tissue-specific manner.
361 HOXB13 is upregulated in breast cancer, whereas its expression is suppressed in
362 prostate cancer (41, 42). HOXD10 is upregulated in breast, gastric, hepatocellular,
363 colorectal, bladder and prostate cancers (43). HOXA9 is upregulated in acute
364 lymphocytic leukaemia and epigenetically silenced in lung cancers (44, 45). HOXA5,
365 HOXA7, HOXA13 and HOXD3 are highly expressed in HCC tissues compared to
366 normal tissues (46). Notably, HOXA13 and HOTTIP were found to be highly expressed
367 in the same neoplastic hepatocyte populations and in liver cancer cell lines (46, 47).
368 HOTTIP, a long noncoding RNA (lncRNA) located contiguous to the HOXA13 gene,
369 directly interacts with WDR5/MLL complexes to induce an open chromatin
370 configuration by driving histone H3 Lys 4 trimethylation, leading to the induction of
371 HOXA genes, including HOXA13 (48); moreover, HOXA13 can induce the
372 transcription of HOTTIP as well as genes related to cell growth and cell invasion (47,
373 49). High expression of both HOTTIP and HOXA13 was correlated with metastasis
374 formation and poor patient survival in HCC, suggesting that HOTTIP/HOXA13
375 expression may be a possible marker for predicting clinical outcomes in HCC patients
376 (47). Although HCV infection cannot potently induce HOXA13 gene transcription in
377 Huh7OK1 cells (10), the discrepancies in the data between our previous study and the
378 abovementioned *in vivo* study may be due to the high expression of HOXA13/HOTTIP
379 in the Huh7 cell line, regardless of the HCV infection status (47). Another lncRNA,
380 HOTAIRM1, was also reported to induce the expression of HOXA1, which could

381 promote the expression of Nanog (50). Some HOX genes associated with
382 carcinogenesis may be constitutively expressed via a positive feedback loop in
383 hepatocytes after DAA treatment.
384 In this study, HCV infection reduced the level of RNF2 and reactivated the
385 expression of silenced HOX genes. However, some clinical reports suggest that the
386 RNF2 and HOX proteins are highly expressed in cancer tissues (51). The data presented
387 in this study may reflect the status of HCV-infected hepatocytes during the early stage
388 and before the premalignant state of liver cancer but not during the malignant state of
389 liver cancer. The expression of some HOX genes has been reported to be maintained in
390 the malignant state of HCC regardless of the high expression of PRC1 components,
391 including RNF2 and PCGF4 (BMI1), suggesting that the expression of some HOX
392 genes may be regulated by factors other than PRC1, such as lncRNAs (e.g., HOTTIP,
393 described above), regardless of the high RNF2 activity at the malignant stage of HCC.
394 Increased expression of RNF2 in HCC tissue was reported to synergistically regulate
395 crosstalk among the histone modifications H2Aub, H3K27me3 and H3Kme3 to
396 suppress E-cadherin transcription (52). HCV infection increases the RNF2 mRNA level
397 but reduces the RNF2 protein level in HCV-infected hepatocytes (10) and may
398 subsequently irreversibly trigger RNF2 transcription, which may be maintained even
399 after viral eradication at the malignant stage of HCC.
400 The possibility remains that PA28γ activation in HCV-infected cells may be
401 associated with viral particle production in these cells. The data presented in our early
402 work revealed that PA28γ knockdown reduced the production of HCV viral particles in
403 the supernatant but did not affect viral RNA replication (21). In this study, compared
404 with that in wild-type cells, the core protein level was much higher in either infected or
405 core protein-expressing PA28γ-knockout cells (Fig. 6A, 7A), while PA28γ knockout
406 reduced the infectious titre in the culture supernatant but did not affect viral RNA
407 replication (Fig. 6C). Nonfunctional or unfolded core proteins were reported to interact
408 with PA28γ for their proteasome-dependent degradation (20, 53). A functional core
409 protein may be engulfed by a nonfunctional or an unfolded core protein in the absence
410 of PA28γ to suppress viral particle production. Alternatively, a reduction in PRC1
411 activity may affect the expression of host genes related to membrane trafficking or viral
412 assembly. Further study is required to clarify the mechanism by which depletion of
413 PA28γ reduces the production of infectious HCV particles.

414 An increasing number of studies have suggested that the PA28γ proteasome is
415 associated with several kinds of viral infections. Coxsackievirus B3 infection was found
416 to promote PA28γ-mediated proteolysis of p53 (54), suggesting that p53 degradation
417 increases viral replication by reducing the inhibitory influence of p53 on viral
418 replication. On the other hand, PA28γ-dependent proteasome activity was associated
419 with an inhibitory effect on viral replication. Ko et al reported that PA28γ acted as a
420 corepressor of human T-lymphotropic virus 1 (HTLV-1) p30 and was required for the
421 suppression of viral replication and maintenance of viral latency (55). Regarding
422 hepatitis B virus (HBV) infection, PA28γ was reported to be associated with HBV
423 pathogenesis. The HBV X protein (HBx) activates HBV promoters to increase HBV
424 RNA transcription, increase the abundance of covalently closed circular DNA
425 (cccDNA) and promote the degradation of the host protein Smc5/6, which can inhibit
426 HBV replication (56, 57). HBx plays an important oncogenic role in the liver in
427 hepatitis B patients (58). For example, HBx promotes the expression of PA28γ to
428 degrade p16 to promote progression through the G1 and M phases (59). In addition,
429 PA28γ stabilizes the HBx protein by competitively inhibiting the binding of HBx to
430 Siah-1 (60). HBx was reported to be polyubiquitinated by Siah-1 for proteasome-
431 dependent degradation (61), and PA28γ competitively inhibited the binding of Siah-1 to
432 HBx, leading to an increase in HBx stability. Thus, PA28γ may be an attractive target
433 for the treatment of hepatitis B and C as well as other viral diseases.
434 In summary, our data presented herein indicate that HCV infection or core protein
435 expression reinforces the interaction between CBP and PA28γ and promotes PA28γ
436 acetylation and heptamerization to activate the proteasome for RNF2 degradation and
437 that a reduction in the RNF2 protein level impairs the monoubiquitination of histone
438 H2A at K119 in the promoter regions of HOX alleles. The reactivation of silenced HOX
439 genes may be associated with HCV-related hepatocellular carcinogenesis. PRC1-
440 dependent histone H2A monoubiquitination silences non-HOX genes (62) and
441 positively or negatively regulates metabolic and developmental gene expression in
442 association with RNA polymerase (63). HCV infection may lead to regulatory effects
443 on various genes via the PCR1-H2Aub pathway during acute and/or chronic infection.
444 Thus, elucidating the mechanism by which HCV infection can regulate PRC1 activity to
445 regulate genes other than HOX genes is important for clarifying the molecular

446 mechanism of hepatitis C pathogenesis and for the development of therapies for
447 hepatitis C.
448
449 **MATERIALS AND METHODS**
450 ***Cell lines, HCV strain.***
451 The HCV strain JFH-1, which belongs to genotype 2a (64), was used as the cell culture-
452 adapted HCV (HCVcc) strain in this study. The viral RNA encoded in the plasmid
453 pJFH1 was transcribed and introduced into Huh7 OK1 cells according to the method
454 reported by Wakita et al. (64). The cell infection procedure was reported previously (10)
455 and is described in detail in each figure legend. The Huh7 OK1 cell line, a subclone
456 derived from Huh-7 cells that is highly permissive to infection with the JFH-1 strain,
457 was cultured as reported previously (65). The human embryonic kidney 293T cell line
458 was purchased from the American Type Culture Collection (Manassas, VA, USA). The
459 lysine deacetylase inhibitor TSA and KAT inhibitor C646 were purchased from Sigma–
460 Aldrich Japan (Tokyo, Japan).
461
462 **Plasmids.**
463 The gene encoding PA28γ was subcloned and inserted into the pGBKT7 vector
464 (resulting in the pGBKT7PA28γ plasmid). N-terminal HA-tagged RNF1 or RNF2 was
465 amplified by polymerase chain reaction (PCR) from human liver cDNA using *KOD*
466 DNA polymerase (TOYOBO, Osaka, Japan) and was then inserted into pCAGGS-PM3.
467 The DNA fragment encoding PA28γ was cloned and inserted into pEF pGKpuro and
468 pEF FLAG Gs pGKpuro as reported previously, with the resulting plasmids designated
469 pEF PA28γ and pEF FLAG-PA28γ, respectively (21), as well as into pEGFP-C3
470 (Clontech Takara, Tokyo, Japan). The plasmid encoding the HCV core protein (amino
471 acids 1-192) was used for cloning and insertion of the corresponding DNA into
472 pCAGGS-PM3 as described previously, and the resulting plasmid was designated
473 pCAG-Core (21). N-terminal FLAG-tagged CBP/p300 cDNA was amplified by PCR
474 and was then inserted into pcDNA3.1 (Invitrogen Thermo, Carlsbad, CA).
475
476 ***Yeast two-hybrid screening.***
477 The bait plasmid pGBKT7PA28γ was introduced into *Saccharomyces*
478 *cerevisiae* AH109 cells. Yeast cells containing pGBKT7PA28γ were grown in yeast

479 extract-peptone-dextrose medium and transfected with a human foetal brain plasmid
480 library based on pACT2 (Clontech Takara). Clones ($22.4 \times 10^6$) generated with the
481 library were screened (Clontech Takara, Tokyo, Japan). Yeast clones containing
482 pGBKT7-53 and pGADT7-T (Clontech) were used as positive controls, while yeast
483 clones containing pGBKT7 and pGADT7 were used as negative controls. Yeast
484 colonies grown on dropout plates lacking tryptophan, leucine, histidine, and adenine
485 were inoculated on two fresh dropout plates lacking leucine and tryptophan. One of the
486 two plates was used for a β-galactosidase assay according to the method of Duttweiller
487 (66), and the other plate was stored at 4 °C as a master plate. One of the 556 dropout
488 plate-positive clones exhibited dark blue staining on a β-galactosidase assay plate to the
489 same extent as the positive control and was called C1-26. The plasmid in Cl-26 cells
490 encoded the RNF1 gene. We amplified the genes encoding RNF1 and the RNF1
491 homologue RNF2 from the total human liver cDNA by PCR and then inserted the
492 sequences into several plasmids as described above. We also isolated the yeast clone
493 encoding PA28γ by this screening method, which supported the accuracy of this
494 screening method.
495
496 ***Transfection, immunoblotting, immunoprecipitation, and gene silencing.***
497 Plasmid DNA was transfected into Huh7OK1 or 293T cells by using TransIT®-LT1
498 (Mirus Bio, Madison, WI). Lysate preparation and immunoprecipitation were carried
499 out as described previously (21). The cell lysates were subjected to 5-20% sodium
500 dodecyl sulfate–polyacrylamide gel electrophoresis (SDS–PAGE) for standard protein
501 analysis or to native PAGE using a NativePAGE™ 3–12% mini protein gel and a
502 Sample Prep Kit (Thermo Fisher) for analysis of the heptamerization of PA28γ. The
503 proteins in the gel were transferred onto polyvinylidene difluoride membranes (Merck
504 Millipore, Billerica, MA). After protein transfer, the membranes were incubated first
505 with an appropriate primary antibody and then with a horseradish peroxidase-
506 conjugated rabbit or mouse IgG as a secondary antibody, immersed in Super Signal
507 West Femto (Thermo Fisher Scientific, Rockford, IL) and visualized using an LAS
508 4000 Mini imaging system (Cytiva, Marlborough, MA). The small interfering RNAs
509 (siRNAs) targeting RNF2 and the control siRNA (siControl Non-targeting siRNA #2,
510 Dharmacon®) were purchased from Thermo Scientific (Brebières, France) and were
511 introduced into cells by using Lipofectamine RNAiMax (Thermo Fisher Scientific). The

512 Silencer® siRNAs with ID numbers s3495 and s3497 were purchased from Thermo
513 Fisher Scientific and are designated CBP#1 and siCBP#2, respectively, in this study.
514 The CHX chase assay was carried out by the method reported by Kao et al (67).
515
516 ***Reverse transcription–quantitative polymerase chain reaction (RT–qPCR) and***
517 ***reverse transcription–semiquantitative polymerase chain reaction (RT–sqPCR).***
518 Total RNA and first-strand cDNA were prepared and then evaluated by RT–qPCR as
519 described previously (10). The expression levels of HCV RNA and of each host mRNA
520 were normalized to that of GAPDH mRNA. HCV RNA and GAPDH mRNA were
521 amplified using primer pairs as described previously (21, 65). Each PCR product was
522 confirmed to be detected as a single band of the correct size by agarose gel
523 electrophoresis. The amount of HCV in the culture supernatant was estimated as the
524 copy number (10). HOX gene mRNA levels were measured by RT–sqPCR or RT–
525 qPCR (68) using the appropriate primer pairs as described previously (10). Takara
526 Emerald (2x;Takara Co.) was used for RT–sqPCR. Data acquisition was performed for
527 25, 30, 35, and 40 cycles to confirm that the plateau phase had not been reached.
528
529 ***Evaluation of immunofluorescence staining in cells by microscopy.***
530 Huh7OK1 wild-type or transfected cells were infected with HCVcc, passaged twice
531 every 4 days, seeded at $0.5 \times 10^4$ cells per well on a glass cover slip and incubated at
532 37 °C for 24 h. The cells were washed twice with phosphate-buffered saline (PBS) and
533 fixed with 4% paraformaldehyde at room temperature for 20 min. After fixation, the
534 cells were washed twice with PBS, permeabilized by incubation for 15 min at room
535 temperature in PBS containing 0.3% saponin, and then incubated in PBS containing 3%
536 bovine serum albumin (PBS-BSA) to block nonspecific signals. These cells were
537 stained with 50 μM DAPI and incubated at 4 °C overnight in PBS-BSA containing
538 rabbit anti-RNF2 IgG (clone D22F2, Cell Signaling Technology, Denver, MA) and
539 mouse anti-NS5A IgG (clone 9E10) or rabbit anti-H2Aub IgG (clone D27C4, Cell
540 Signaling Technology) and mouse anti-HCV core protein IgG (clone B2, ANOGEN,
541 Mississauga, Canada). The cells were washed three times with PBS-BSA and incubated
542 at room temperature for 2 h in PBS-BSA containing appropriate Alexa Fluor (AF)-
543 conjugated secondary antibodies (Thermo Fisher Scientific). The cells were washed
544 three times with PBS-BSA and observed using a confocal laser scanning microscope

545 (FV1000, Olympus, Tokyo) or fluorescence microscope (BZ-9000 and BZ-X800:
546 Keyence, Osaka, Japan). The core-positive and core-negative areas were determined
547 and evaluated using fluorescence microscopy and corresponding software (BZ-H4:
548 Keyence, Osaka, Japan).
549
550 ***ChIP assay.***
551 ChIP assays were carried out according to the method reported by Sakurai et al (69)
552 with modifications as described previously (10). Huh7OK1 cells were infected with
553 HCVcc and passaged twice every 4 days. HCV-infected cells and mock-infected cells
554 were harvested 8 dpi. DNA–protein complexes were prepared as described previously
555 (10). qPCR was carried out as described above without a reverse transcription step.
556
557 ***Gene knockout with the CRISPR/Cas9 system.***
558 PA28γ-knockout Huh7OK1 cell lines were established according to the method
559 reported by Fujihara et al. (70). A PA28γ-targeting sequence (5'-
560 ATGGGATGCTGAAAAGCAAC -3') was used for the construction of the pX330
561 plasmid encoding the guide RNA. The targeted DNA regions were amplified from the
562 genomic DNA of Huh7OK1 cells with the primer pair 5'-
563 ACTGAGGATCCATGTTTTAGACGCTCATCTGTAGTTC-3'/5'-
564 GATATCGAATTCCAACCCAGGAGGCAGAGGTC-3' and were subsequently
565 inserted into pCAG EGxxFP. Both pX330 and pCAG EGxxFP were purchased from
566 Addgene (Cat Nos. #42230 and #50716; Cambridge, MA). Huh7OK1 cells were
567 transfected with these plasmids using Lipofectamine LTX (Thermo Fisher Scientific).
568 GFP-positive cells were isolated using a FACSAria$^{TM}$ cell sorter (BD Bioscience) 48 h
569 post-transfection. Single-cell clones were established by a colony isolation technique.
570 The deleted regions of each allele of the PA28γ gene were confirmed by direct
571 sequencing. The PA28γ mRNA transcribed from each allele in the PA28γ-knockout cell
572 line was expected to lack the sequence 5'-GCTGAAAAGCAACCAGCAGCT or
573 ACCAGCAGCTG-3'. The expression of PA28γ was confirmed by immunoblot
574 analysis.
575
576 ***In vitro proteasome assay***

577 The plasmids encoding HA-RNF1 and HA-RNF2 were transfected into PA28γ-
578 knockout Huh7OK1 cells (5 x $10^5$ cells) and then harvested 48 hr. The cell lysates were
579 prepared in 1 ml of NP-40 Lysis buffer (50 mM Tris 7.4 pH, 150 mM NaCl, 1% NP-40,
580 10% glycerol, 1x protease inhibitor cocktail). HA-RNF1 or HA-RNF2 was then isolated
581 by immunoprecipitation using an anti-HA antibody for *in vitro* proteasome assays.
582 The in vitro proteasome assay was conducted using purified 20S proteasome (Enzo Life
583 Science, Farmingdale, NY) and proteasome activator 11S γ subunit (Enzo Life
584 Science). The immunoprecipitates containing HA-RNF1 or HA-RNF2 (one-twentieth of
585 the total immunoloprecipitates) were mixed on ice with 20S CP (50 ng protein) with or
586 without the 11S PA consisting of PA28γ (28 ng protein) in proteasome assay buffer (25
587 mM Tris-HCl pH7.4, 10% glycerol, 10 mM $MgCl_2$, 1 mM DTT, 2 mM ATP). The
588 mixture was incubated at 37 ˚C and stopped at 0, 10 or 30 min by boiling after adding
589 SDS-sample buffer. The resulting mixtures were analysed by Western blotting. Intensity
590 of RNF1 and RNF2 protein signals were measured using Image Gauge software (GE
591 health care).
592
593 ***Statistical analysis.***
594 The measured values are shown as the means ± standard deviations (SDs). The
595 statistical significance of differences in the means was determined by Student's *t* test.
596
597 **Acknowledgements**
598 We thank T. Wakita, F. V. Chisari and R. Bartenschlager for providing plasmids and
599 cell lines. We also thank M. Mori for her secretarial work and C. Endoh for technical
600 assistance. This work was supported by Grants-in-Aid from the Japan Agency for
601 Medical Research and Development (24fk0210109), JST Moonshot R&D
602 (JPMJMS2025), and scholarship donations from Teijin Co. Ltd and Yakult Co., Ltd.
603

604 **Figure legends.**

605 **FIG 1: PA28γ could bind RNF2 but was not colocalized with RNF2.**

606 (A) FLAG-PA28γ was expressed in 293T cells together with HA-RNF1 or HA-RNF2.
607 The cells were harvested 48 h post-transfection. These cell lysates were subjected to
608 immunoprecipitation. Immunoprecipitates recovered with anti-HA or anti-FLAG
609 antibodies were analysed by Western blotting using anti-FLAG or anti-HA antibodies,
610 respectively. (B) The intracellular localization of PA28γ and RNF2 was examined by
611 immunocytofluorescence. Images were acquired with a Keyence fluorescence
612 microscope. (C) The image in the field of view shown in the top of panel C was
613 acquired with a fluorescence microscope and subjected to three-dimensional
614 reconstruction. The green and red fluorescence intensities in each pixel (in coordinate
615 form) were calculated using the analysis software. The data shown in this figure are
616 representative of three independent experiments.

617

618 **FIG 2. The endogenous RNF2 protein was stabilized by genetic knockout of**
619 **PA28γ.**

620 (A) PA28γ gene knockout was conducted using the Huh7OK1 cell line and the
621 CRISPR-Cas9 system. PA28γ was detected in the parental cells but not in the PA28γ-
622 knockout cells. PA28γ-knockout Huh7OK1 cells or parental Huh7OK1 cells
623 (Huh7OK1) were treated with the translation inhibitor CHX (2 mg/ml). Endogenous
624 RNF1, RNF2 and BMI1 expression was evaluated by Western blotting. (B) The band
625 densities of RNF1, RNF2, BMI1 and β-actin shown in panel A were estimated using
626 ImageJ software. The values for RNF1, RNF2 and BMI1 were normalized to that of β-
627 actin and are presented as percentages with respect to those in mock-infected cells. The
628 data shown in this figure are representative of three independent experiments and are
629 presented as the means ± SDs (n = 3). **: $p < 0.01$.

630

631 **FIG 3. RNF2 degradation was promoted by the expression of PA28γ.**

632 (A) PA28γ-knockout Huh7OK1 cells were transfected with pEF PA28γ (0, 0.03, 0.1
633 and 0.3 μg/sample) or the empty vector. The total amount of transfected DNA in pEF
634 PA28γ-transfected cells was supplemented with the empty plasmid to a final amount of
635 0.3 μg per sample. Endogenous RNF1, RNF2, BMI1, PA28γ and β-actin expression
636 was evaluated by Western blotting. (B) Total RNA was prepared from the harvested

637 cells described in panel A. The levels of RNF1 mRNA and RNF2 mRNA were
638 estimated via RT–qPCR. These mRNA levels were normalized to the GAPDH mRNA
639 level and are presented as relative values compared to the empty plasmid control. The
640 data shown in this figure are representative of three independent experiments and are
641 presented as the means ± SDs (n =3). (C) PA28γ-knockout Huh7OK1 cells were
642 transfected with pEF PA28γ (0, 0.03, 0.1 and 0.3 μg/sample) or the empty vector
643 together with the plasmid encoding HA-RNF1 or HA-RNF2 (0.2 μg/sample). The total
644 amount of transfected DNA in pEF PA28γ-transfected cells was supplemented with the
645 empty plasmid to a final amount of 0.5 μg per sample. (D) The immuno-precipitates
646 including HA-RNF1 or HA-RNF2 were mixed with 20S CP and 11S PA (PA28γ) in the
647 reaction buffer and then incubated at 0, 10 or 30 min. The resulting preparations were
648 subjected into Western blotting. The data shown in this figure are representative of three
649 independent experiments.
650
651 **FIG 4. The degradation of the RNF2 protein and the reduction in H2Aub were**
652 **promoted by PA28γ and suppressed by proteasome inhibition.**
653 (A) PA28γ-knockout Huh7OK1 cells were transfected with pEF PA28γ and treated with
654 10 μM MG132 at 48 h post-transfection. The resulting cells were harvested at 52 h post-
655 transfection. These cell lysates were subjected to Western blotting. (B) The cells
656 described in panel A were fixed and stained with the appropriate antibodies as described
657 in the Materials and Methods. The intracellular localization of RNF2 and PA28γ was
658 observed via confocal laser scanning microscopy. (C) PA28γ-knockout cells were
659 transfected with plasmids encoding PA28γ or PA28γP245Y. The resulting cells were
660 fixed 48 h post-transfection and stained with appropriate antibodies as described in the
661 Materials and Methods. The nuclear localization of RNF2 and PA28γ was observed via
662 confocal laser scanning microscopy. The images were subjected to three-dimensional
663 reconstruction. The green and red fluorescence intensities in each pixel (in coordinate
664 form) were calculated using the analysis software. The data shown in this figure are
665 representative of three independent experiments.
666
667 **FIG 5. PA28γ was required for the induction of HOX genes.**
668 (A) PA28γ-knockout Huh7OK1 cells were transfected with pEF PA28γ (0, 0.1, 0.3 and
669 1.0 μg/sample) or the empty vector. The total amount of transfected DNA in these cells

670 was supplemented with the empty plasmid to a final amount of 1.0 μg per sample.
671 These cells were treated with 10 μM MG132 at 48 h post-transfection and were then
672 harvested at 52 h post-transfection. These cell lysates were subjected to Western
673 blotting. (B and D) Total RNA was prepared from the harvested cells described in panel
674 A. The level of each HOX mRNA was estimated via RT–qPCR. These mRNA levels
675 were normalized to the GAPDH mRNA level and are presented as relative values
676 compared to the empty plasmid control. The data shown in this figure are representative
677 of three independent experiments and are presented as the means ± SDs (n =3). (C) The
678 level of H2Aub in the promoter region of HOXB9 was evaluated by a chromatin
679 immunoprecipitation (ChIP) assay. The data shown in this figure are representative of
680 three independent experiments and are presented as the means ± SDs (n =3).
681
682 **FIG 6. HCV infection reduced the levels of H2Aub and RNF2 in the presence but**
683 **not in the absence of PA28γ.**
684 Huh7OK1 cells (WT) and PA28γ-knockout Huh7OK1 cells (PA28γKO) were infected
685 with HCVcc at m.o.i. of 0.5 and harvested at 0, 3 and 6 dpi. These cell lysates were
686 subjected to Western blotting (A), and the band densities of H2Aub and RNF2 were
687 estimated by a method similar to that described in Figs. 2 and 5 (B). The levels of
688 cellular and supernatant HCV RNA were estimated by RT–qPCR, and the infectivity in
689 the supernatant was estimated by a focus formation assay (C). The data shown in this
690 figure are representative of three independent experiments and are presented as the
691 means ± SDs (n =3).
692
693 **FIG 7. HCV core protein expression reduced the levels of H2Aub and RNF2 in the**
694 **presence but not in the absence of PA28γ.**
695 (A) PA28γ-knockout Huh7OK1 cells (PA28γKO) and the parental cells (WT) were
696 transfected with pCAG Core (0, 0.1, 0.3 and 1.0 μg/sample) or the empty vector. The
697 total amount of transfected DNA in these cells was supplemented with the empty
698 plasmid to a final amount of 1.0 μg per sample. These cell lysates were subjected to
699 Western blotting. The data shown in this figure are representative of three independent
700 experiments. (B) The cells described in panel A were subjected to a ChIP assay to
701 estimate the level of H2Aub in the promoter region of HOXB9. The data shown in this
702 figure are representative of three independent experiments and are presented as the

703 means ± SDs (n =3). (C) Total RNA was prepared from the cells described in panel A.
704 The level of HOXB9 mRNA was estimated by RT–qPCR. The data shown in this figure
705 are representative of three independent experiments and are presented as the
706 means ± SDs (n =3).
707
708 **FIG 8: Acetylation of PA28γ at K195 was essential for the reduction in the RNF2**
709 **protein level.**
710 (A and B) PA28γ-knockout HuhOK1 cells were transfected with pEF PA28γ or the
711 empty vector and were then treated with C646 and CHX at 36 h post-transfection. The
712 cells were collected at 42 h post-transfection. These cell lysates were subjected to
713 Western blotting. (C and D) PA28γ-knockout HuhOK1 cells were transfected with pEF
714 PA28γ or the empty vector and were then treated with TSA at 36 h post-transfection.
715 The cells were collected at 0, 2 and 4 h posttreatment. These cell lysates were subjected
716 to Western blotting. (E) PA28γ, PA28γ K195R or PA28γK195Q were expressed in
717 PA28γ-knockout Huh7OK1 cells. The transfected cells were treated with CHX and
718 harvested at 0, 2 and 6 h posttreatment. These cell lysates were subjected to Western
719 blotting. (F) Huh7OK1 cells were transfected with pCAG Core (0, 0.3 and 1.0
720 μg/sample) or the empty vector. The total amount of transfected DNA in these cells was
721 supplemented with the empty plasmid to a final amount of 1.0 μg per sample. The cells
722 were treated with CHX at 36 h post-transfection and harvested at 42 h post-transfection.
723 These cell lysates were subjected to Western blotting.
724
725 **FIG 9. HCV core proteins induce the acetylation and activation of PA28γ via the**
726 **KAT CBP, leading to a decrease in the RNF2 protein level.**
727 (A) Parental Huh7OK1 cells and PA28γ-knockout Huh7OK1 cells were infected with
728 HCVcc at an m.o.i. of 0.5 and harvested at 0, 3 and 6 dpi. These cell lysates were
729 subjected to immunoprecipitation using rabbit anti-Ace-K IgG or normal rabbit IgG.
730 The resulting precipitates and cell lysates were subjected to Western blotting. (B) The
731 cell lysates described in panel A were subjected to Western blotting to analyse the
732 formation of PA28γ heptamers. (C) PA28γ-knockout Huh7OK1 cells were transfected
733 with pEF PA28γ (0.3 μg/sample) and/or pCAG Core (0.3 μg/sample). Total DNA was
734 supplemented with the empty plasmid to a final amount of 1.0 μg per sample. The cells
735 were harvested at 48 h post-transfection. These cell lysates were subjected to

736 immunoprecipitation using rabbit anti-Ace-K IgG or normal rabbit IgG. The resulting
737 precipitates and cell lysates were subjected to Western blotting. (D) The cell lysates
738 described in panel C were subjected to Western blotting to analyse the formation of
739 PA28γ heptamers. (E) PA28γ-knockout Huh7OK1 cells were transfected with pEGFP
740 PA28γ (0.3 μg/sample), pcDNA3.1 FLAG-CBP (0.3 μg/sample), and/or pCAG Core
741 (0.3 μg/sample). Total DNA was supplemented with the empty plasmid to a final
742 amount of 1.0 μg per sample. The cells were harvested at 48 h post-transfection. The
743 resulting cell lysates were subjected to immunoprecipitation and Western blotting. (E)
744 Huh7OK1 cells were transfected with control siRNA (c), siCBP#1 (#1) or siCBP#2
745 (#2). The transfected cells were infected at 16 h post-transfection with HCVcc at an
746 m.o.i. of 0.5. The infected cells were harvested at 3 dpi. The resulting cell lysates were
747 subjected to Western blotting.
748
749 **FIG 10. Schematic diagram of the mechanism by which HCV infection**
750 **accelerates the activation of the PA28γ-20S CP complex for the degradation of**
751 **RNF2, the reduction in H2Aub, and the induction of HOX genes.**
752 Most HOX alleles are silenced in uninfected hepatocytes (10). When hepatocytes are
753 infected with HCV, the core protein reinforces the interaction between CBP and PA28γ
754 to increase PA28γ acetylation and heptamerization. The PA28γ heptamer recruits RNF2
755 and activates the 20S CP to degrade RNF2. The degradation of RNF2 results in a
756 decrease in PRC1 activity and impairs the monoubiquitination of histone H2A. The
757 reduction in H2Aub results in the formation of open chromatin in the promoter regions
758 of HOX alleles and the transcriptional reactivation of silenced HOX genes.
759
760 **REFERENCES**
761
762 1. WHO. 2024. Fact sheet: Hepatitis C, *on* World Health Organization.
763 https://www.who.int/news-room/fact-sheets/detail/hepatitis-c. Accessed
764 2. Marshall AD, Willing AR, Kairouz A, Cunningham EB, Wheeler A, O'Brien N, Perera
765 V, Ward JW, Hiebert L, Degenhardt L, Hajarizadeh B, Colledge S, Hickman M, Jawad
766 D, Lazarus JV, Matthews GV, Scheibe A, Vickerman P, Dore GJ, Grebely J, Global
767 HCV, Group HIVTR. 2024. Direct-acting antiviral therapies for hepatitis C infection:

768 global registration, reimbursement, and restrictions. Lancet Gastroenterol Hepatol
769 9:366-382.
770 3. Rinaldi L, Nevola R, Franci G, Perrella A, Corvino G, Marrone A, Berretta M, Morone
771 MV, Galdiero M, Giordano M, Adinolfi LE, Sasso FC. 2020. Risk of Hepatocellular
772 Carcinoma after HCV Clearance by Direct-Acting Antivirals Treatment Predictive
773 Factors and Role of Epigenetics. Cancers (Basel) 12.
774 4. Moriishi K. 2017. The potential of signal peptide peptidase as a therapeutic target for
775 hepatitis C. Expert Opin Ther Targets 21:827-836.
776 5. Shintani Y, Fujie H, Miyoshi H, Tsutsumi T, Tsukamoto K, Kimura S, Moriya K,
777 Koike K. 2004. Hepatitis C virus infection and diabetes: direct involvement of the virus
778 in the development of insulin resistance. Gastroenterology 126:840-8.
779 6. Moriya K, Yotsuyanagi H, Shintani Y, Fujie H, Ishibashi K, Matsuura Y, Miyamura T,
780 Koike K. 1997. Hepatitis C virus core protein induces hepatic steatosis in transgenic
781 mice. J Gen Virol 78 ( Pt 7):1527-31.
782 7. Roingeard P, Hourioux C. 2008. Hepatitis C virus core protein, lipid droplets and
783 steatosis. J Viral Hepat 15:157-64.
784 8. Mahmoudvand S, Shokri S, Taherkhani R, Farshadpour F. 2019. Hepatitis C virus core
785 protein modulates several signaling pathways involved in hepatocellular carcinoma.
786 World J Gastroenterol 25:42-58.
787 9. Moriya K, Fujie H, Shintani Y, Yotsuyanagi H, Tsutsumi T, Ishibashi K, Matsuura Y,
788 Kimura S, Miyamura T, Koike K. 1998. The core protein of hepatitis C virus induces
789 hepatocellular carcinoma in transgenic mice. Nat Med 4:1065-7.
790 10. Kasai H, Mochizuki K, Tanaka T, Yamashita A, Matsuura Y, Moriishi K. 2021.
791 Induction of HOX Genes by Hepatitis C Virus Infection via Impairment of Histone
792 H2A Monoubiquitination. J Virol 95:01784-20.
793 11. Carnesecchi J, Pinto PB, Lohmann I. 2018. Hox transcription factors: an overview of
794 multi-step regulators of gene expression. Int J Dev Biol 62:723-732.
795 12. Feng Y, Zhang T, Wang Y, Xie M, Ji X, Luo X, Huang W, Xia L. 2021. Homeobox
796 Genes in Cancers: From Carcinogenesis to Recent Therapeutic Intervention. Front
797 Oncol 11:770428.
798 13. Wang H, Wang L, Erdjument-Bromage H, Vidal M, Tempst P, Jones RS, Zhang Y.
799 2004. Role of histone H2A ubiquitination in Polycomb silencing. Nature 431:873-8.

800 14. Thomas T, Salcedo-Tacuma D, Smith DM. 2023. Structure, Function, and Allosteric
801 Regulation of the 20S Proteasome by the 11S/PA28 Family of Proteasome Activators.
802 Biomolecules 13.
803 15. Thomas TA, Smith DM. 2022. Proteasome activator 28gamma (PA28gamma)
804 allosterically activates trypsin-like proteolysis by binding to the alpha-ring of the 20S
805 proteasome. J Biol Chem 298:102140.
806 16. Li X, Lonard DM, Jung SY, Malovannaya A, Feng Q, Qin J, Tsai SY, Tsai MJ,
807 O'Malley BW. 2006. The SRC-3/AIB1 coactivator is degraded in a ubiquitin- and ATP-
808 independent manner by the REGgamma proteasome. Cell 124:381-92.
809 17. Uchimura Y, Barton LF, Rada C, Neuberger MS. 2011. REG-gamma associates with
810 and modulates the abundance of nuclear activation-induced deaminase. J Exp Med
811 208:2385-91.
812 18. Chen X, Barton LF, Chi Y, Clurman BE, Roberts JM. 2007. Ubiquitin-independent
813 degradation of cell-cycle inhibitors by the REGgamma proteasome. Mol Cell 26:843-
814 52.
815 19. Paesen GC, Nuttall PA. 1996. A tick homologue of the human Ki nuclear autoantigen.
816 Biochim Biophys Acta 1309:9-13.
817 20. Moriishi K, Okabayashi T, Nakai K, Moriya K, Koike K, Murata S, Chiba T, Tanaka K,
818 Suzuki R, Suzuki T, Miyamura T, Matsuura Y. 2003. Proteasome activator
819 PA28gamma-dependent nuclear retention and degradation of hepatitis C virus core
820 protein. J Virol 77:10237-49.
821 21. Moriishi K, Shoji I, Mori Y, Suzuki R, Suzuki T, Kataoka C, Matsuura Y. 2010.
822 Involvement of PA28gamma in the propagation of hepatitis C virus. Hepatology
823 52:411-20.
824 22. Miyamoto H, Moriishi K, Moriya K, Murata S, Tanaka K, Suzuki T, Miyamura T,
825 Koike K, Matsuura Y. 2007. Involvement of the PA28gamma-dependent pathway in
826 insulin resistance induced by hepatitis C virus core protein. J Virol 81:1727-35.
827 23. Moriishi K, Mochizuki R, Moriya K, Miyamoto H, Mori Y, Abe T, Murata S, Tanaka
828 K, Miyamura T, Suzuki T, Koike K, Matsuura Y. 2007. Critical role of PA28gamma in
829 hepatitis C virus-associated steatogenesis and hepatocarcinogenesis. Proc Natl Acad Sci
830 U S A 104:1661-6.

831 24. Murata S, Kawahara H, Tohma S, Yamamoto K, Kasahara M, Nabeshima Y, Tanaka K,
832 Chiba T. 1999. Growth retardation in mice lacking the proteasome activator
833 PA28gamma. J Biol Chem 274:38211-5.
834 25. Huang L, Haratake K, Miyahara H, Chiba T. 2016. Proteasome activators, PA28gamma
835 and PA200, play indispensable roles in male fertility. Sci Rep 6:23171.
836 26. Li L, Zhao D, Wei H, Yao L, Dang Y, Amjad A, Xu J, Liu J, Guo L, Li D, Li Z, Zuo D,
837 Zhang Y, Liu J, Huang S, Jia C, Wang L, Wang Y, Xie Y, Luo J, Zhang B, Luo H,
838 Donehower LA, Moses RE, Xiao J, O'Malley BW, Li X. 2013. REGgamma deficiency
839 promotes premature aging via the casein kinase 1 pathway. Proc Natl Acad Sci U S A
840 110:11005-10.
841 27. Okamoto T, Nishimura Y, Ichimura T, Suzuki K, Miyamura T, Suzuki T, Moriishi K,
842 Matsuura Y. 2006. Hepatitis C virus RNA replication is regulated by FKBP8 and
843 Hsp90. EMBO J 25:5015-5025.
844 28. Zhang Z, Clawson A, Realini C, Jensen CC, Knowlton JR, Hill CP, Rechsteiner M.
845 1998. Identification of an activation region in the proteasome activator REGalpha. Proc
846 Natl Acad Sci U S A 95:2807-11.
847 29. Geng Z, Gao Z. 2020. Mammalian PRC1 Complexes: Compositional Complexity and
848 Diverse Molecular Mechanisms. Int J Mol Sci 21.
849 30. Zhou W, Zhu P, Wang J, Pascual G, Ohgi KA, Lozach J, Glass CK, Rosenfeld MG.
850 2008. Histone H2A monoubiquitination represses transcription by inhibiting RNA
851 polymerase II transcriptional elongation. Mol Cell 29:69-80.
852 31. Zhu P, Zhou W, Wang J, Puc J, Ohgi KA, Erdjument-Bromage H, Tempst P, Glass CK,
853 Rosenfeld MG. 2007. A histone H2A deubiquitinase complex coordinating histone
854 acetylation and H1 dissociation in transcriptional regulation. Mol Cell 27:609-21.
855 32. Liu J, Wang Y, Li L, Zhou L, Wei H, Zhou Q, Liu J, Wang W, Ji L, Shan P, Wang Y,
856 Yang Y, Jung SY, Zhang P, Wang C, Long W, Zhang B, Li X. 2013. Site-specific
857 acetylation of the proteasome activator REGgamma directs its heptameric structure and
858 functions. J Biol Chem 288:16567-16578.
859 33. Gomez-Gonzalo M, Benedicto I, Carretero M, Lara-Pezzi E, Maldonado-Rodriguez A,
860 Moreno-Otero R, Lai MM, Lopez-Cabrera M. 2004. Hepatitis C virus core protein
861 regulates p300/CBP co-activation function. Possible role in the regulation of NF-AT1
862 transcriptional activity. Virology 328:120-30.

863 34. Domovitz T, Gal-Tanamy M. 2021. Tracking Down the Epigenetic Footprint of HCV-
864 Induced Hepatocarcinogenesis. J Clin Med 10.
865 35. Chen Y, Ji H, Shao J, Jia Y, Bao Q, Zhu J, Zhang L, Shen Y. 2020. Different Hepatitis
866 C Virus Infection Statuses Show a Significant Risk of Developing Type 2 Diabetes
867 Mellitus: A Network Meta-Analysis. Dig Dis Sci 65:1940-1950.
868 36. Shiu TY, Huang SM, Shih YL, Chu HC, Chang WK, Hsieh TY. 2013. Hepatitis C virus
869 core protein down-regulates p21(Waf1/Cip1) and inhibits curcumin-induced apoptosis
870 through microRNA-345 targeting in human hepatoma cells. PLoS One 8:e61089.
871 37. Chang PC, Chi CW, Chau GY, Li FY, Tsai YH, Wu JC, Wu Lee YH. 2006. DDX3, a
872 DEAD box RNA helicase, is deregulated in hepatitis virus-associated hepatocellular
873 carcinoma and is involved in cell growth control. Oncogene 25:1991-2003.
874 38. Chang ML, Chen TH, Chang MY, Yeh CT. 2009. Cell cycle perturbation in the
875 hepatocytes of HCV core transgenic mice following common bile duct ligation is
876 associated with enhanced p21 expression. J Med Virol 81:467-72.
877 39. Li X, Amazit L, Long W, Lonard DM, Monaco JJ, O'Malley BW. 2007. Ubiquitin- and
878 ATP-independent proteolytic turnover of p21 by the REGgamma-proteasome pathway.
879 Mol Cell 26:831-42.
880 40. Gong D, Zhu H, Zeng L, Hu R, Hu J, Ding J. 2021. Overexpression of HOXA10
881 promotes the growth and metastasis of nasopharyngeal carcinoma. Exp Biol Med
882 (Maywood) 246:2454-2462.
883 41. Wang Z, Dahiya S, Provencher H, Muir B, Carney E, Coser K, Shioda T, Ma XJ, Sgroi
884 DC. 2007. The prognostic biomarkers HOXB13, IL17BR, and CHDH are regulated by
885 estrogen in breast cancer. Clin Cancer Res 13:6327-34.
886 42. Jung C, Kim RS, Lee SJ, Wang C, Jeng MH. 2004. HOXB13 homeodomain protein
887 suppresses the growth of prostate cancer cells by the negative regulation of T-cell factor
888 4. Cancer Res 64:3046-51.
889 43. Surendran H, Palaniyandi T, Natarajan S, Hari R, Viwanathan S, Baskar G, Abdul
890 Wahab MR, Ravi M, Rajendran BK. 2023. Role of homeobox d10 gene targeted
891 signaling pathways in cancers. Pathol Res Pract 248:154643.
892 44. Faber J, Krivtsov AV, Stubbs MC, Wright R, Davis TN, van den Heuvel-Eibrink M,
893 Zwaan CM, Kung AL, Armstrong SA. 2009. HOXA9 is required for survival in human
894 MLL-rearranged acute leukemias. Blood 113:2375-85.

895 45. Rauch T, Wang Z, Zhang X, Zhong X, Wu X, Lau SK, Kernstine KH, Riggs AD,
896 Pfeifer GP. 2007. Homeobox gene methylation in lung cancer studied by genome-wide
897 analysis with a microarray-based methylated CpG island recovery assay. Proc Natl
898 Acad Sci U S A 104:5527-32.
899 46. Cillo C, Schiavo G, Cantile M, Bihl MP, Sorrentino P, Carafa V, M DA, Roncalli M,
900 Sansano S, Vecchione R, Tornillo L, Mori L, De Libero G, Zucman-Rossi J,
901 Terracciano L. 2011. The HOX gene network in hepatocellular carcinoma. Int J Cancer
902 129:2577-87.
903 47. Quagliata L, Quintavalle C, Lanzafame M, Matter MS, Novello C, di Tommaso L,
904 Pressiani T, Rimassa L, Tornillo L, Roncalli M, Cillo C, Pallante P, Piscuoglio S, Ng
905 CK, Terracciano LM. 2018. High expression of HOXA13 correlates with poorly
906 differentiated hepatocellular carcinomas and modulates sorafenib response in in vitro
907 models. Lab Invest 98:95-105.
908 48. Wang KC, Yang YW, Liu B, Sanyal A, Corces-Zimmerman R, Chen Y, Lajoie BR,
909 Protacio A, Flynn RA, Gupta RA, Wysocka J, Lei M, Dekker J, Helms JA, Chang HY.
910 2011. A long noncoding RNA maintains active chromatin to coordinate homeotic gene
911 expression. Nature 472:120-4.
912 49. Wong CH, Li CH, He Q, Chan SL, Tong JH, To KF, Lin LZ, Chen Y. 2020. Ectopic
913 HOTTIP expression induces noncanonical transactivation pathways to promote growth
914 and invasiveness in pancreatic ductal adenocarcinoma. Cancer Lett 477:1-9.
915 50. Li F, Xu Y, Xu X, Ge S, Zhang F, Zhang H, Fan X. 2020. lncRNA HotairM1 Depletion
916 Promotes Self-Renewal of Cancer Stem Cells through HOXA1-Nanog Regulation
917 Loop. Mol Ther Nucleic Acids 22:456-470.
918 51. Yan Q, Chen BJ, Hu S, Qi SL, Li LY, Yang JF, Zhou H, Yang CC, Chen LJ, Du J.
919 2021. Emerging role of RNF2 in cancer: From bench to bedside. J Cell Physiol
920 236:5453-5465.
921 52. Yao L, Li J, Jiang B, Zhang Z, Li X, Ouyang X, Xiao Y, Liu G, Wang Z, Zhang G.
922 2023. RNF2 inhibits E-Cadherin transcription to promote hepatocellular carcinoma
923 metastasis via inducing histone mono-ubiquitination. Cell Death Dis 14:261.
924 53. Suzuki R, Moriishi K, Fukuda K, Shirakura M, Ishii K, Shoji I, Wakita T, Miyamura T,
925 Matsuura Y, Suzuki T. 2009. Proteasomal turnover of hepatitis C virus core protein is
926 regulated by two distinct mechanisms: a ubiquitin-dependent mechanism and a
927 ubiquitin-independent but PA28gamma-dependent mechanism. J Virol 83:2389-92.

928 54. Gao G, Wong J, Zhang J, Mao I, Shravah J, Wu Y, Xiao A, Li X, Luo H. 2010.
929 Proteasome activator REGgamma enhances coxsackieviral infection by facilitating p53
930 degradation. J Virol 84:11056-66.
931 55. Ko NL, Taylor JM, Bellon M, Bai XT, Shevtsov SP, Dundr M, Nicot C. 2013.
932 PA28gamma is a novel corepressor of HTLV-1 replication and controls viral latency.
933 Blood 121:791-800.
934 56. Decorsiere A, Mueller H, van Breugel PC, Abdul F, Gerossier L, Beran RK, Livingston
935 CM, Niu C, Fletcher SP, Hantz O, Strubin M. 2016. Hepatitis B virus X protein
936 identifies the Smc5/6 complex as a host restriction factor. Nature 531:386-9.
937 57. Murphy CM, Xu Y, Li F, Nio K, Reszka-Blanco N, Li X, Wu Y, Yu Y, Xiong Y, Su L.
938 2016. Hepatitis B Virus X Protein Promotes Degradation of SMC5/6 to Enhance HBV
939 Replication. Cell Rep 16:2846-2854.
940 58. Levrero M, Zucman-Rossi J. 2016. Mechanisms of HBV-induced hepatocellular
941 carcinoma. J Hepatol 64:S84-S101.
942 59. Cha S, Jang KL. 2020. Hepatitis B virus X protein stimulates cell growth by
943 downregulating p16 levels via PA28gamma-mediated proteasomal degradation. J Gen
944 Virol 101:963-971.
945 60. Han J, Kim H, Jeong H, Yoon H, Jang KL. 2021. Proteasomal activator 28 gamma
946 stabilizes hepatitis B virus X protein by competitively inhibiting the Siah-1-mediated
947 proteasomal degradation. Biochem Biophys Res Commun 578:97-103.
948 61. Yeom S, Kim SS, Jeong H, Jang KL. 2017. Hepatitis B virus X protein activates E3
949 ubiquitin ligase Siah-1 to control virus propagation via a negative feedback loop. J Gen
950 Virol 98:1774-1784.
951 62. Boyer LA, Plath K, Zeitlinger J, Brambrink T, Medeiros LA, Lee TI, Levine SS,
952 Wernig M, Tajonar A, Ray MK, Bell GW, Otte AP, Vidal M, Gifford DK, Young RA,
953 Jaenisch R. 2006. Polycomb complexes repress developmental regulators in murine
954 embryonic stem cells. Nature 441:349-53.
955 63. Brookes E, de Santiago I, Hebenstreit D, Morris KJ, Carroll T, Xie SQ, Stock JK,
956 Heidemann M, Eick D, Nozaki N, Kimura H, Ragoussis J, Teichmann SA, Pombo A.
957 2012. Polycomb associates genome-wide with a specific RNA polymerase II variant,
958 and regulates metabolic genes in ESCs. Cell Stem Cell 10:157-70.
959 64. Wakita T, Pietschmann T, Kato T, Date T, Miyamoto M, Zhao Z, Murthy K,
960 Habermann A, Krausslich HG, Mizokami M, Bartenschlager R, Liang TJ. 2005.

961 Production of infectious hepatitis C virus in tissue culture from a cloned viral genome.
962 Nat Med 11:791-6.
963 65. Kasai H, Kawakami K, Yokoe H, Yoshimura K, Matsuda M, Yasumoto J, Maekawa S,
964 Yamashita A, Tanaka T, Ikeda M, Kato N, Okamoto T, Matsuura Y, Sakamoto N,
965 Enomoto N, Takeda S, Fujii H, Tsubuki M, Kusunoki M, Moriishi K. 2015.
966 Involvement of FKBP6 in hepatitis C virus replication. Sci Rep 5:16699.
967 66. Duttweiler HM. 1996. A highly sensitive and non-lethal beta-galactosidase plate assay
968 for yeast. Trends Genet 12:340-1.
969 67. Kao SH, Wang WL, Chen CY, Chang YL, Wu YY, Wang YT, Wang SP, Nesvizhskii
970 AI, Chen YJ, Hong TM, Yang PC. 2015. Analysis of Protein Stability by the
971 Cycloheximide Chase Assay. Bio Protoc 5.
972 68. Kikuchi K, Kasai H, Watanabe A, Lai AY, Kondo M. 2008. IL-7 specifies B cell fate at
973 the common lymphoid progenitor to pre-proB transition stage by maintaining early B
974 cell factor expression. J Immunol 181:383-92.
975 69. Sakurai N, Inamochi Y, Inoue T, Hariya N, Kawamura M, Yamada M, Dey A,
976 Nishiyama A, Kubota T, Ozato K, Goda T, Mochizuki K. 2017. BRD4 regulates
977 adiponectin gene induction by recruiting the P-TEFb complex to the transcribed region
978 of the gene. Sci Rep 7:11962.
979 70. Fujihara Y, Ikawa M. 2014. CRISPR/Cas9-based genome editing in mice by single
980 plasmid injection. Methods Enzymol 546:319-36.
981

Fig. 1

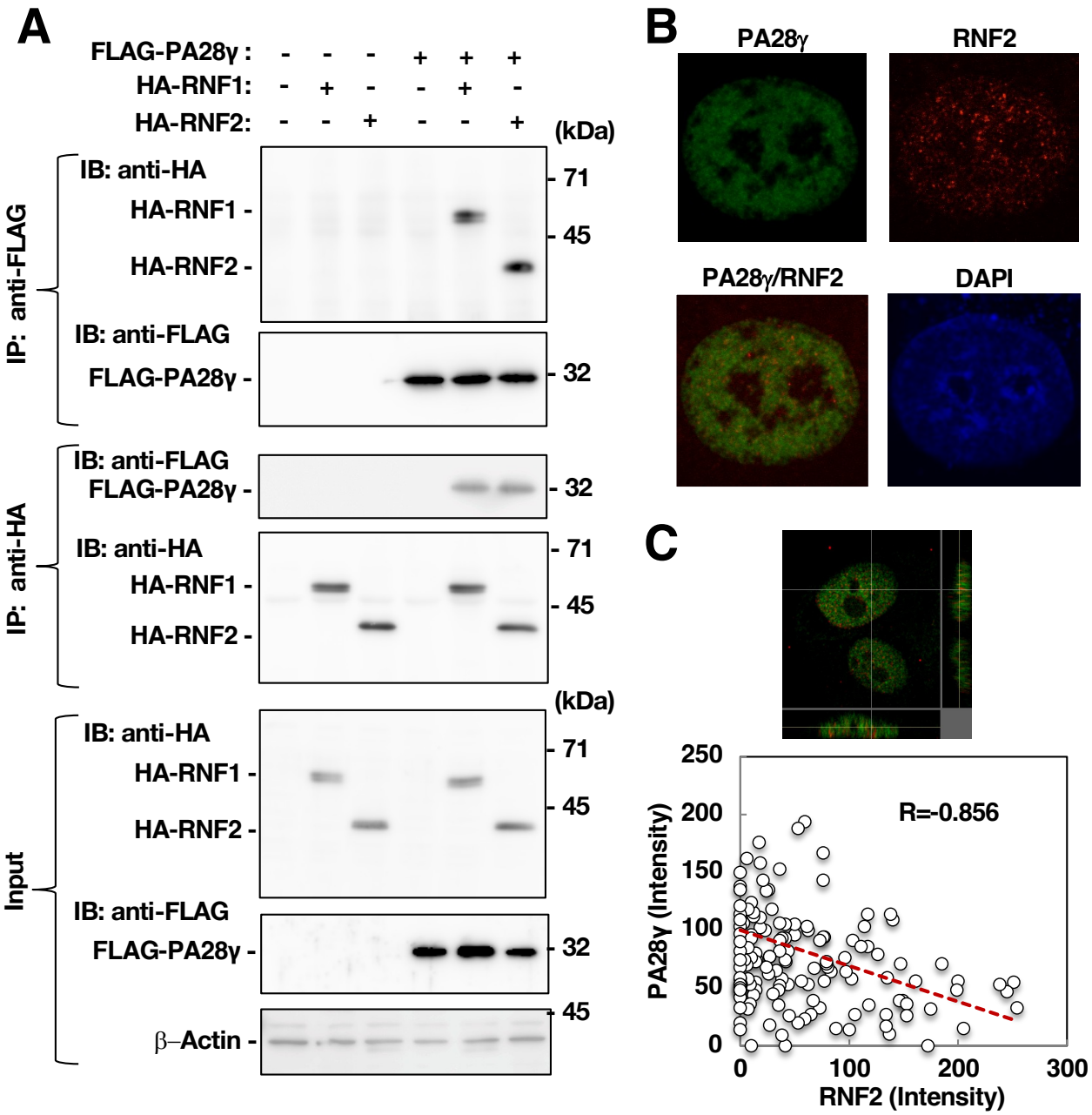
A
FLAG-PA28γ : - - - + + +
HA-RNF1: - + - - + -
HA-RNF2: - - + - - +
(kDa)
IP: anti-FLAG
IB: anti-HA
HA-RNF1 -
HA-RNF2 -
IB: anti-FLAG
FLAG-PA28γ -
71
45
32
IP: anti-HA
IB: anti-FLAG
FLAG-PA28γ -
IB: anti-HA
HA-RNF1 -
HA-RNF2 -
Input
IB: anti-HA
HA-RNF1 -
HA-RNF2 -
IB: anti-FLAG
FLAG-PA28γ -
β–Actin -
B
PA28γ
RNF2
PA28γ/RNF2
DAPI
C
R=-0.856
PA28γ (Intensity)
RNF2 (Intensity)
0
50
100
150
200
250
0
100
200
300

Fig. 2

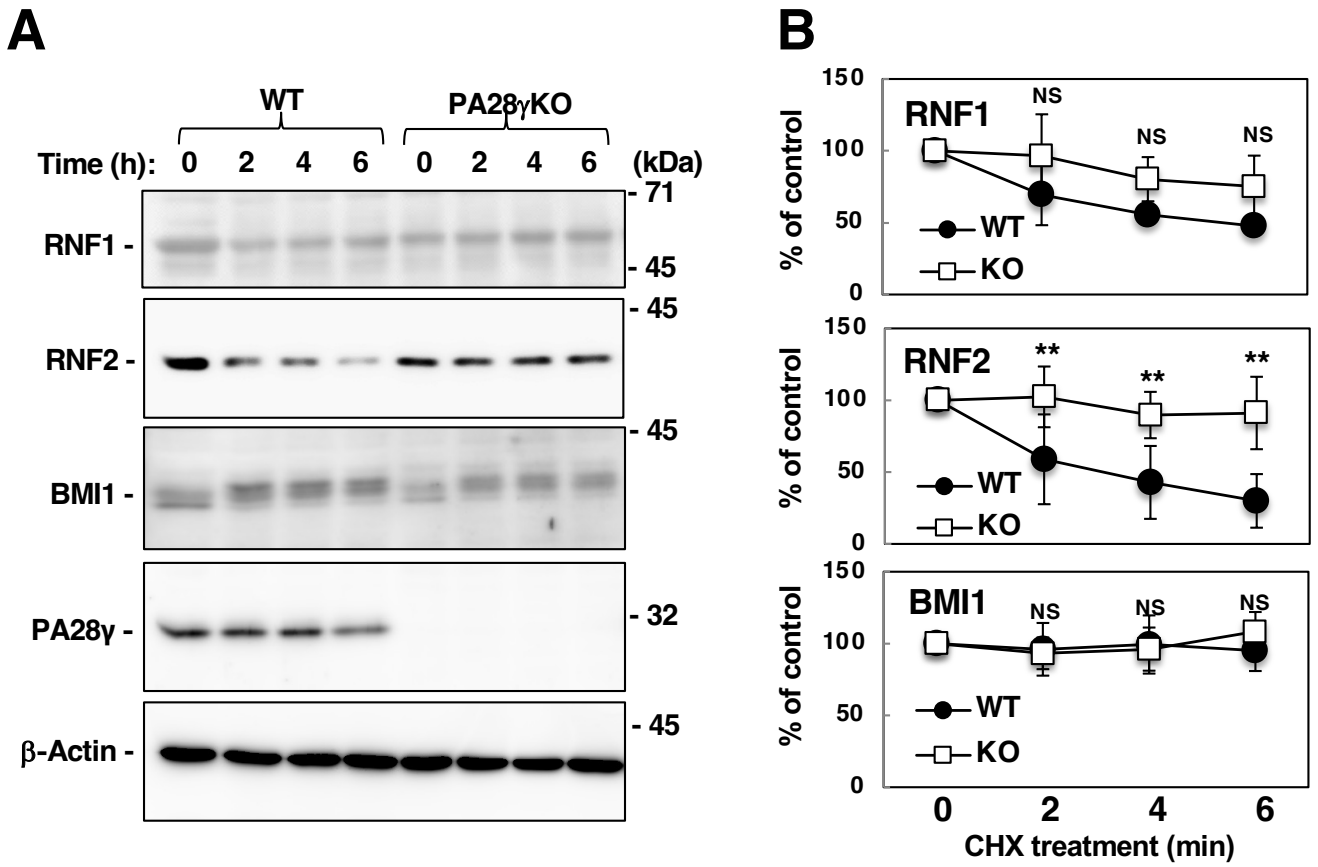
A
WT
PA28γKO
Time (h): 0 2 4 6 0 2 4 6 (kDa)
RNF1 -
- 71
- 45
RNF2 -
- 45
BMI1 -
- 45
PA28γ -
- 32
β-Actin -
- 45
B
RNF1
RNF2
BMI1
% of control
150
100
50
0
NS
**
WT
KO
0 2 4 6
CHX treatment (min)

Fig. 3

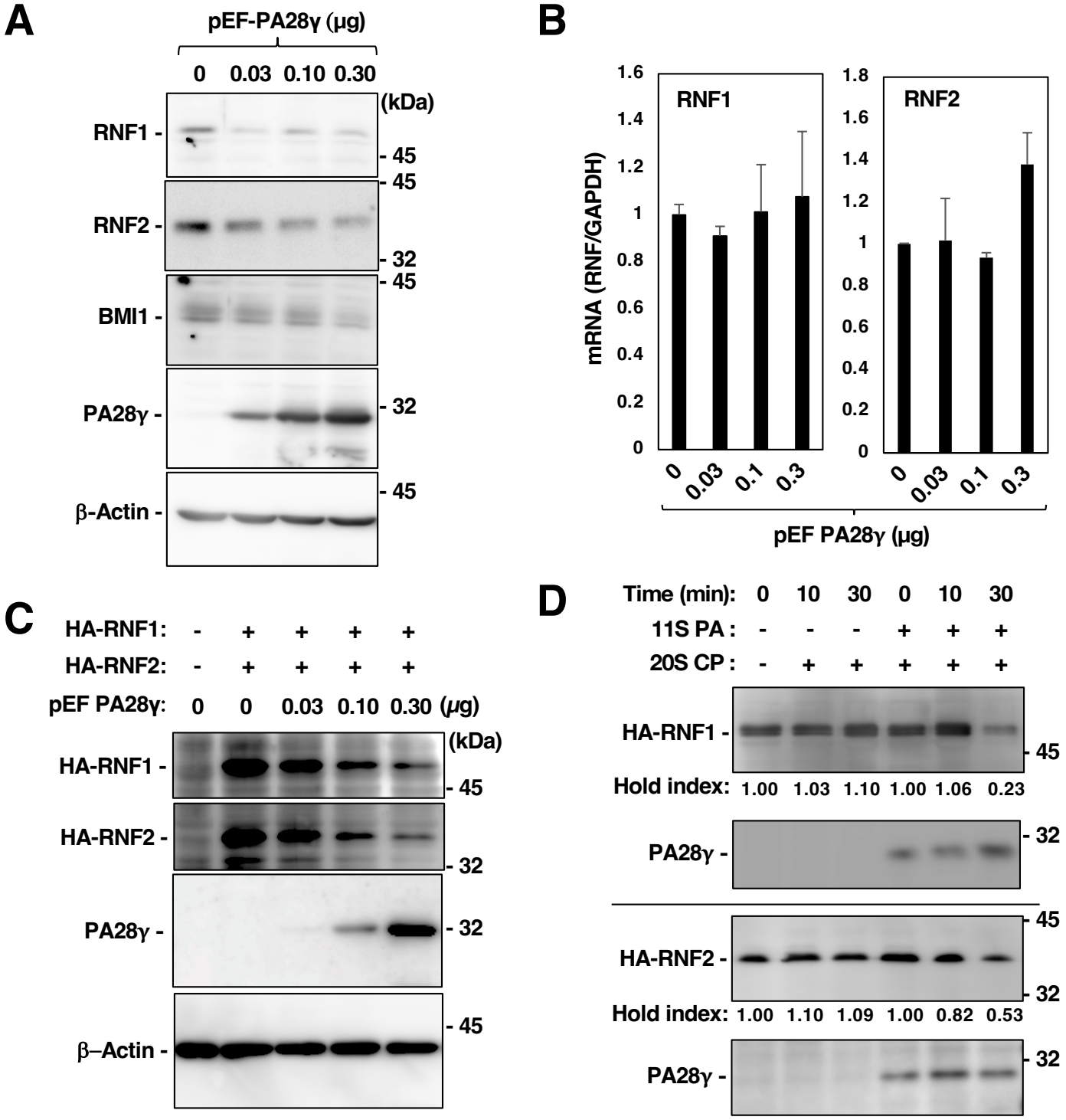
A
pEF-PA28γ (μg)
0 0.03 0.10 0.30
(kDa)
RNF1 -
- 45
RNF2 -
- 45
- 32
BMI1 -
- 45
PA28γ -
- 32
β-Actin -
- 45
B
RNF1
RNF2
mRNA (RNF/GAPDH)
0 0.03 0.1 0.3
pEF PA28γ (μg)
C
HA-RNF1: - + + + +
HA-RNF2: - + + + +
pEF PA28γ: 0 0 0.03 0.10 0.30 (μg)
(kDa)
HA-RNF1 -
- 45
HA-RNF2 -
- 32
PA28γ -
- 32
β–Actin -
- 45
D
Time (min): 0 10 30 0 10 30
11S PA : - - - + + +
20S CP : - + + + + +
HA-RNF1 -
- 45
Hold index: 1.00 1.03 1.10 1.00 1.06 0.23
PA28γ -
- 32
HA-RNF2 -
- 45
- 32
Hold index: 1.00 1.10 1.09 1.00 0.82 0.53
PA28γ -
- 32

Fig. 4

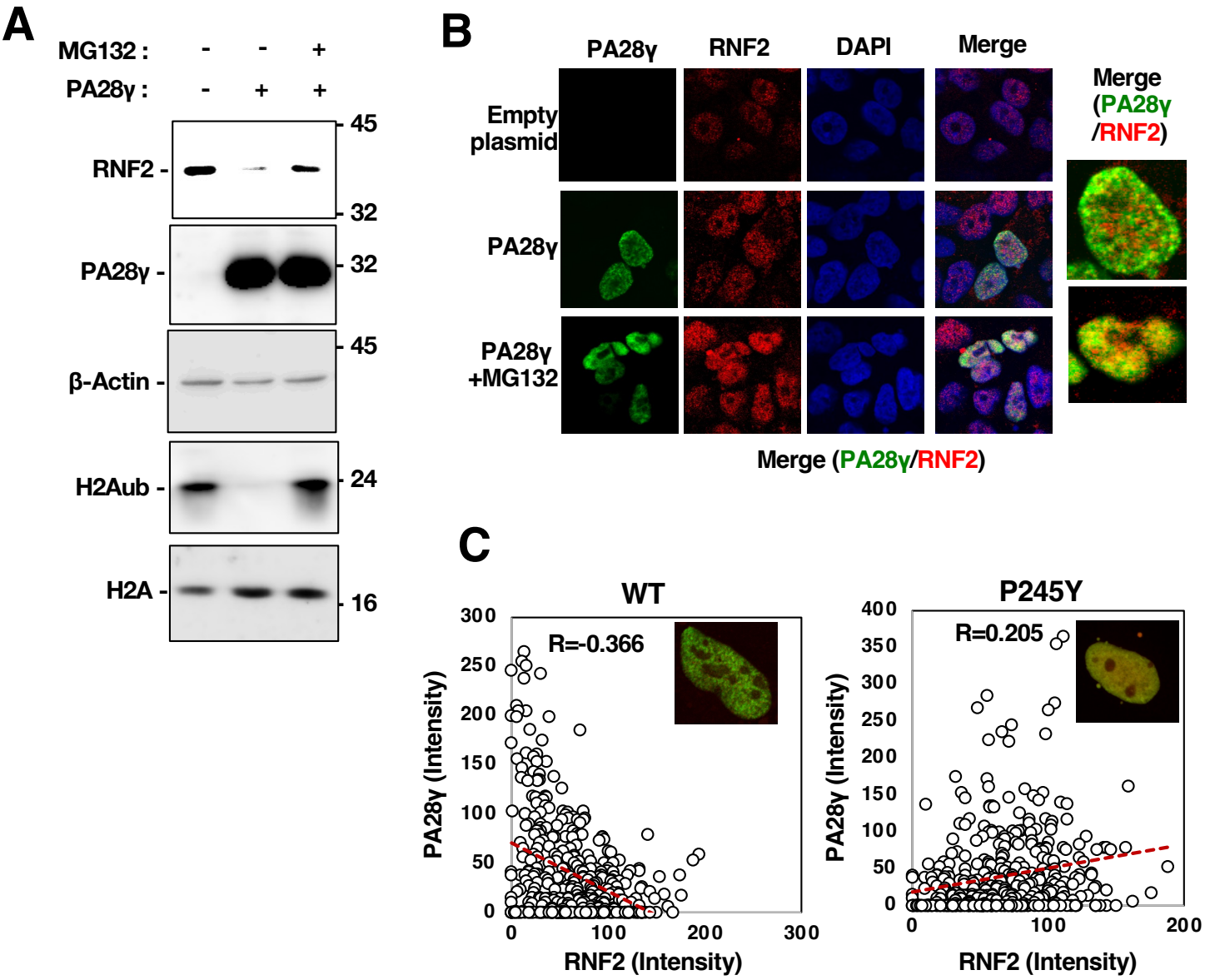
A
MG132 : - - +
PA28γ : - + +
RNF2
PA28γ
β-Actin
H2Aub
H2A
45
32
32
45
24
16
B
PA28γ
RNF2
DAPI
Merge
Merge (PA28γ /RNF2)
Empty plasmid
PA28γ
PA28γ +MG132
Merge (PA28γ/RNF2)
C
WT
R=-0.366
PA28γ (Intensity)
RNF2 (Intensity)
P245Y
R=0.205
PA28γ (Intensity)
RNF2 (Intensity)

Fig. 5

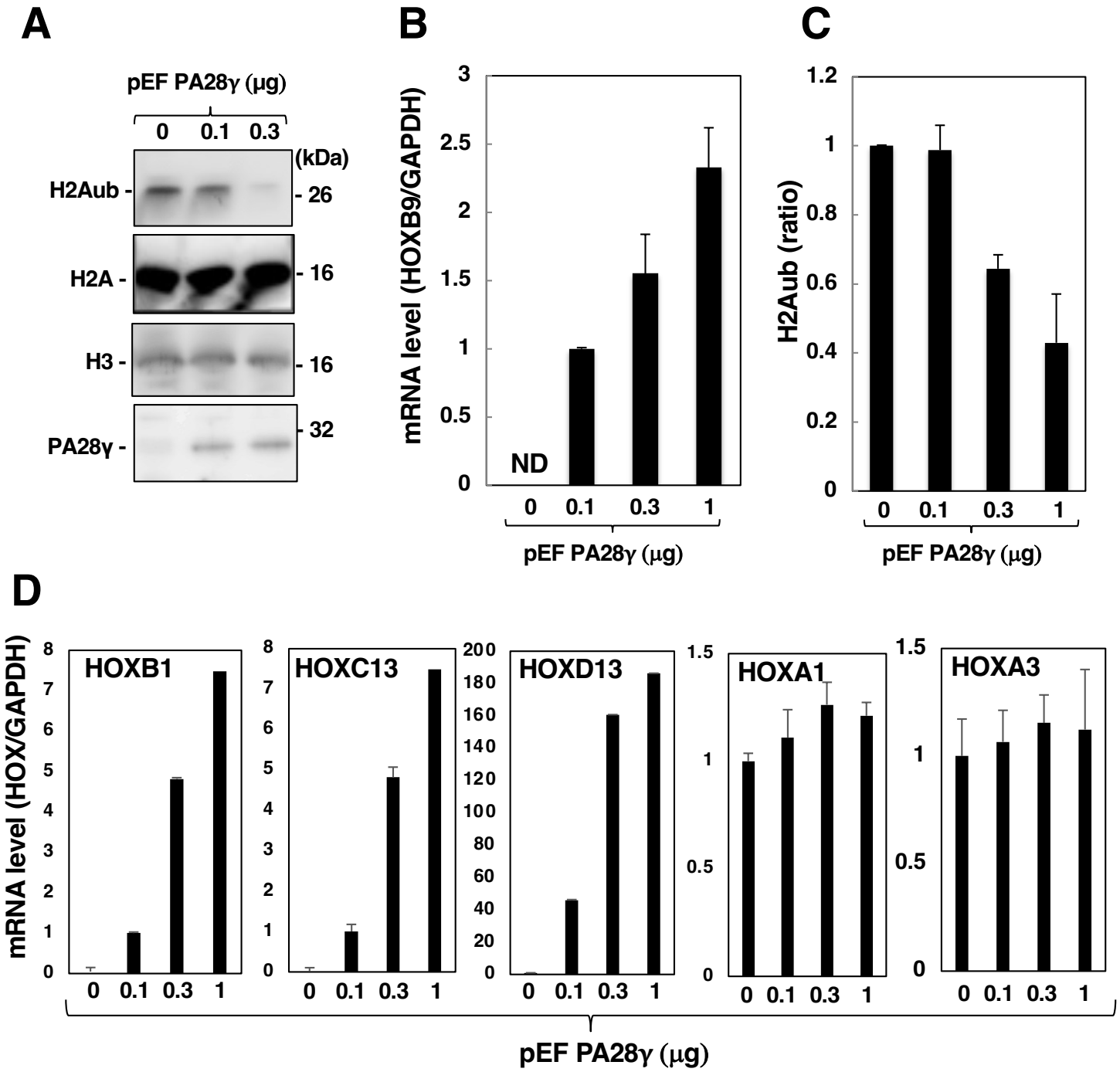
A
pEF PA28γ (μg)
0 0.1 0.3
(kDa)
H2Aub -
- 26
H2A -
- 16
H3 -
- 16
PA28γ -
- 32
B
mRNA level (HOXB9/GAPDH)
ND
0 0.1 0.3 1
pEF PA28γ (μg)
C
H2Aub (ratio)
0 0.1 0.3 1
pEF PA28γ (μg)
D
mRNA level (HOX/GAPDH)
HOXB1
HOXC13
HOXD13
HOXA1
HOXA3
0 0.1 0.3 1
pEF PA28γ (μg)

Fig. 6

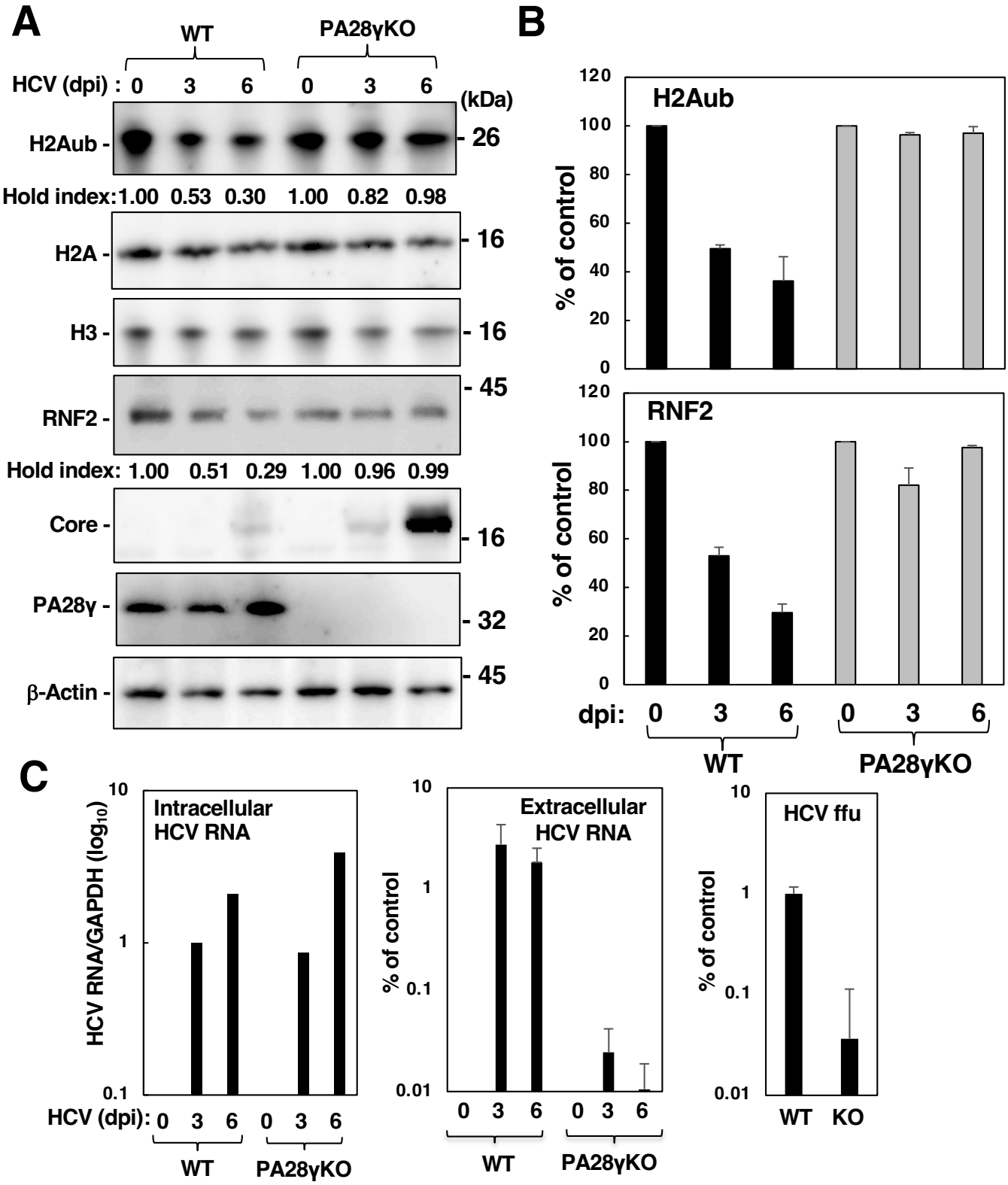
A
WT
PA28γKO
HCV (dpi) : 0 3 6 0 3 6
(kDa)
H2Aub -
- 26
Hold index: 1.00 0.53 0.30 1.00 0.82 0.98
H2A -
- 16
H3 -
- 16
RNF2 -
- 45
Hold index: 1.00 0.51 0.29 1.00 0.96 0.99
Core -
- 16
PA28γ -
- 32
β-Actin -
- 45
B
H2Aub
% of control
RNF2
dpi: 0 3 6 0 3 6
WT
PA28γKO
C
Intracellular HCV RNA
HCV RNA/GAPDH (log10)
HCV (dpi): 0 3 6 0 3 6
WT
PA28γKO
Extracellular HCV RNA
% of control
HCV ffu
WT
KO

Fig. 7

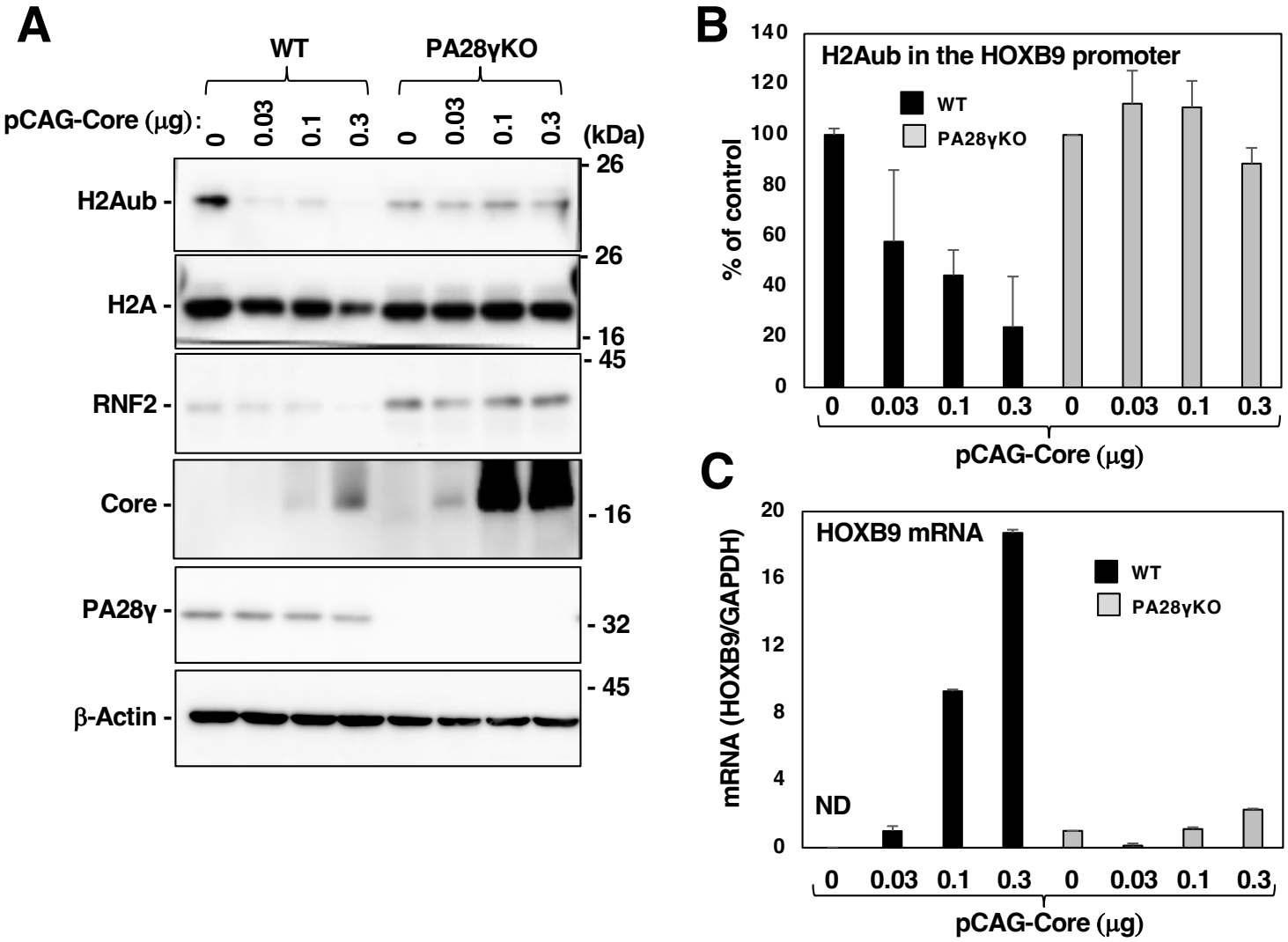
A
WT
PA28γKO
pCAG-Core (μg):
0
0.03
0.1
0.3
0
0.03
0.1
0.3
(kDa)
H2Aub
26
H2A
26
16
RNF2
45
Core
16
PA28γ
32
β-Actin
45
B
H2Aub in the HOXB9 promoter
WT
PA28γKO
% of control
140
120
100
80
60
40
20
0
0
0.03
0.1
0.3
0
0.03
0.1
0.3
pCAG-Core (μg)
C
HOXB9 mRNA
WT
PA28γKO
mRNA (HOXB9/GAPDH)
20
16
12
8
4
0
ND
0
0.03
0.1
0.3
0
0.03
0.1
0.3
pCAG-Core (μg)

Fig. 8

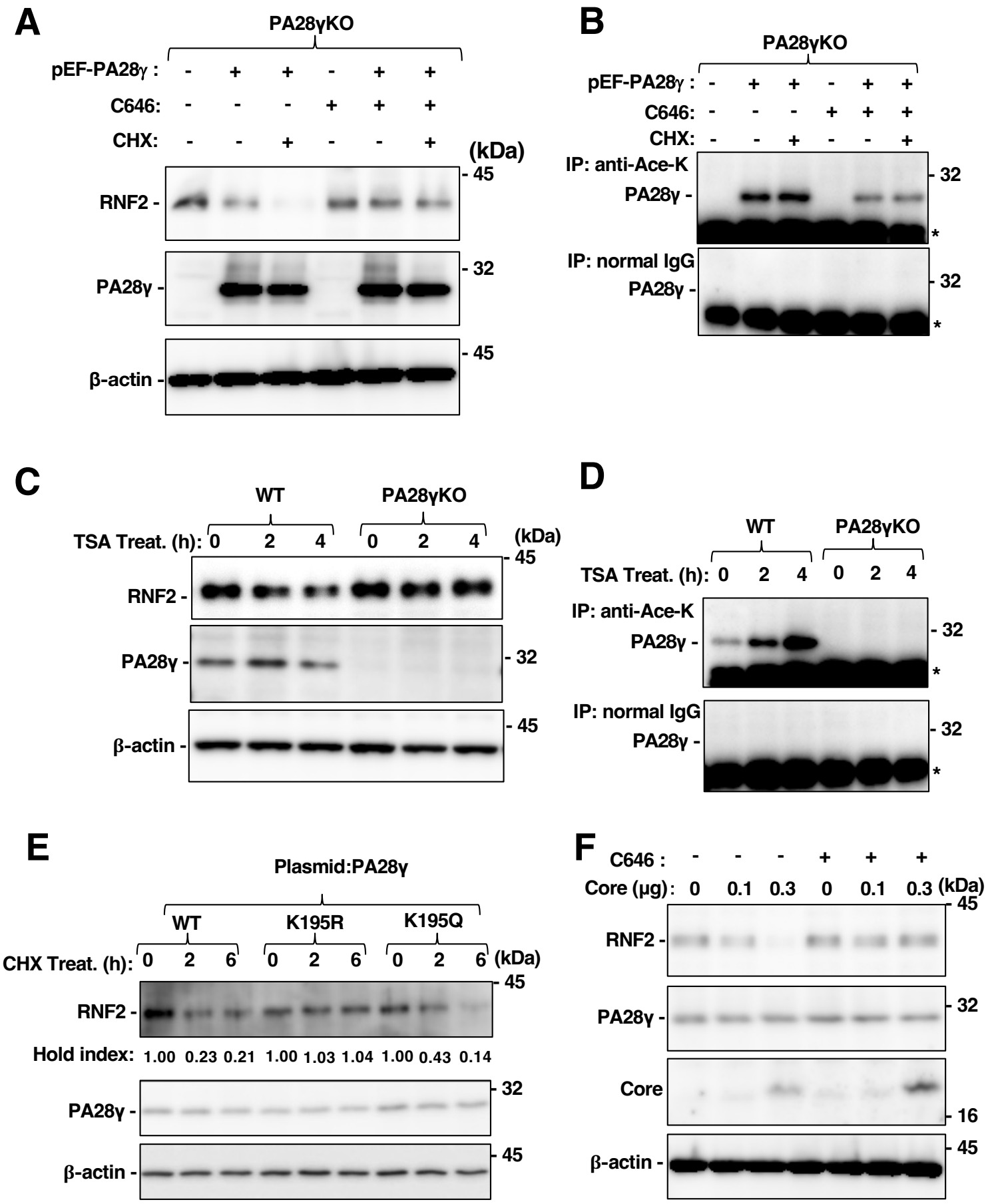
A
PA28γKO
pEF-PA28γ : - + + - + +
C646: - - - + + +
CHX: - - + - - +
(kDa)
RNF2 -
PA28γ -
β-actin -
45
32
45
B
PA28γKO
pEF-PA28γ : - + + - + +
C646: - - - + + +
CHX: - - + - - +
IP: anti-Ace-K
PA28γ -
IP: normal IgG
PA28γ -
32
32
*
*
C
WT
PA28γKO
TSA Treat. (h): 0 2 4 0 2 4
(kDa)
RNF2 -
PA28γ -
β-actin -
45
32
45
D
WT
PA28γKO
TSA Treat. (h): 0 2 4 0 2 4
IP: anti-Ace-K
PA28γ -
IP: normal IgG
PA28γ -
32
32
*
*
E
Plasmid:PA28γ
WT
K195R
K195Q
CHX Treat. (h): 0 2 6 0 2 6 0 2 6
(kDa)
RNF2 -
Hold index: 1.00 0.23 0.21 1.00 1.03 1.04 1.00 0.43 0.14
PA28γ -
β-actin -
45
32
45
F
C646 : - - - + + +
Core (μg): 0 0.1 0.3 0 0.1 0.3
(kDa)
RNF2 -
PA28γ -
Core
β-actin -
45
32
16
45

Fig. 9

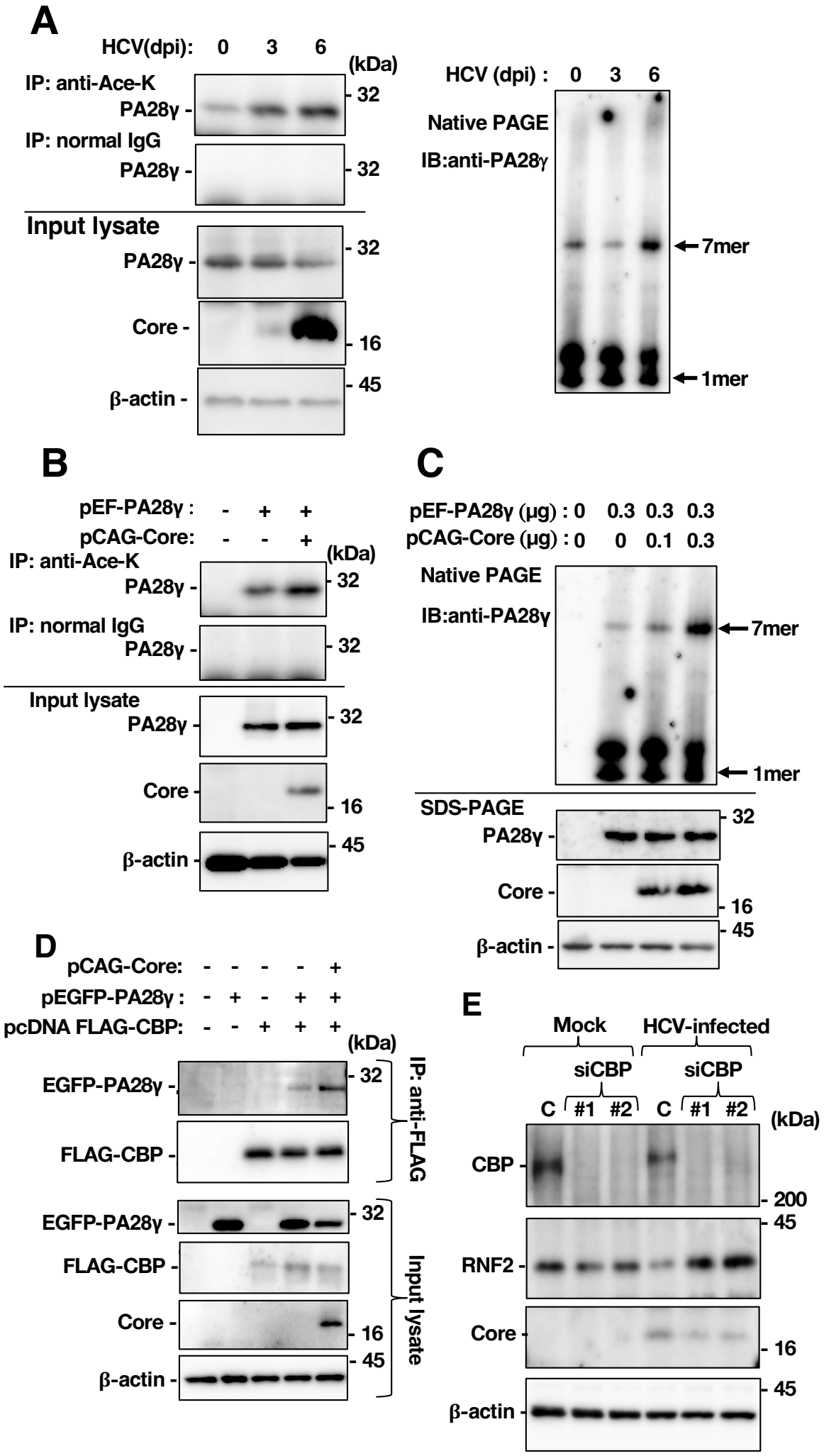
A
HCV(dpi): 0 3 6
(kDa)
IP: anti-Ace-K
PA28γ -
32
IP: normal IgG
PA28γ -
32
Input lysate
PA28γ -
32
Core -
16
β-actin -
45
HCV (dpi) : 0 3 6
Native PAGE
IB:anti-PA28γ
7mer
1mer
B
pEF-PA28γ : - + +
pCAG-Core: - - +
(kDa)
IP: anti-Ace-K
PA28γ -
32
IP: normal IgG
PA28γ -
32
Input lysate
PA28γ -
32
Core -
16
β-actin -
45
C
pEF-PA28γ (μg) : 0 0.3 0.3 0.3
pCAG-Core (μg) : 0 0 0.1 0.3
Native PAGE
IB:anti-PA28γ
7mer
1mer
SDS-PAGE
PA28γ -
32
Core -
16
β-actin -
45
D
pCAG-Core: - - - - +
pEGFP-PA28γ : - + - + +
pcDNA FLAG-CBP: - - + + +
(kDa)
EGFP-PA28γ -
32
FLAG-CBP -
IP: anti-FLAG
EGFP-PA28γ -
32
FLAG-CBP -
Core -
16
β-actin -
45
Input lysate
E
Mock
HCV-infected
siCBP
siCBP
C #1 #2 C #1 #2
(kDa)
CBP -
200
45
RNF2 -
Core -
16
45
β-actin -

Fig. 10

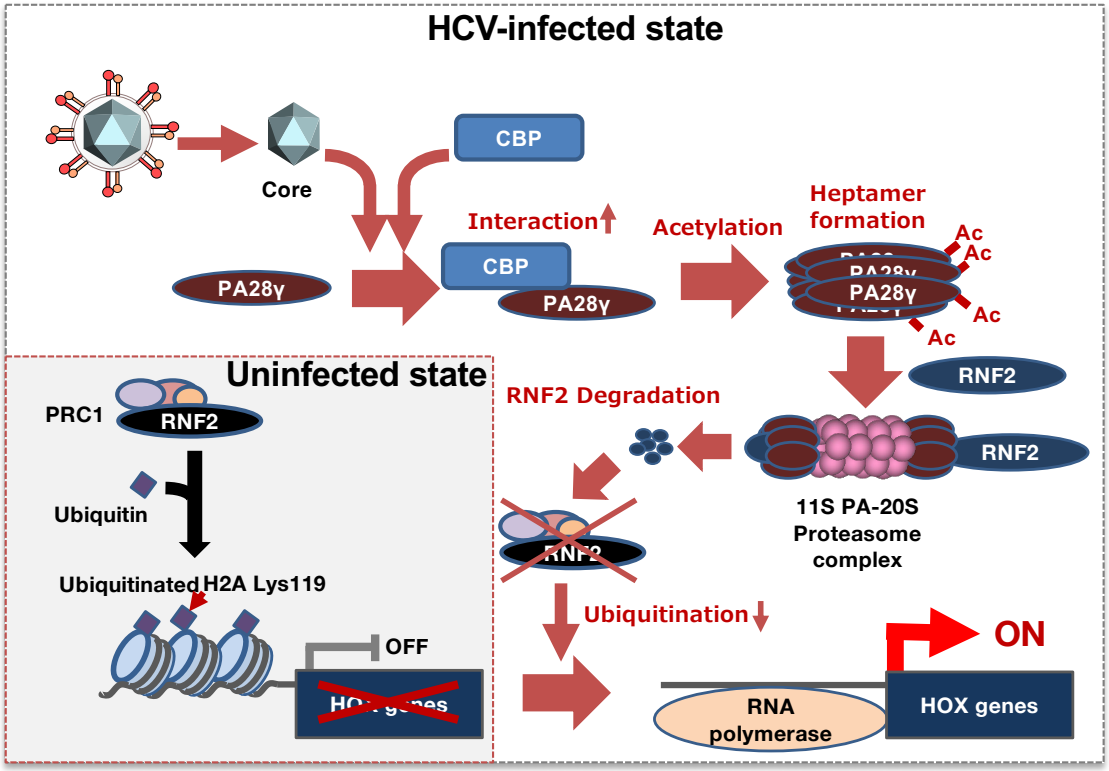
HCV-infected state
Core
CBP
Interaction
Acetylation
Heptamer formation
Ac
Ac
Ac
Ac
PA28γ
CBP
PA28γ
PA28γ
RNF2
RNF2 Degradation
RNF2
11S PA-20S Proteasome complex
Uninfected state
PRC1
RNF2
Ubiquitin
Ubiquitinated H2A Lys119
OFF
Ubiquitination
ON
RNA polymerase
HOX genes